Published in final edited form as:
Brain Behav Immun. 2011 August ; 25(6): 1063–1077. doi:10.1016/j.bbi.2011.03.012.

Voluntary Exercise Protects Hippocampal Neurons from Trimethyltin Injury: Possible Role of Interleukin-6 to Modulate Tumor Necrosis Factor Receptor-Mediated Neurotoxicity

Jason A. Funk[1,#], **Julia Gohlke**[1,2], **Andrew D. Kraft**[1], **Christopher A. McPherson**[1], **Jennifer B. Collins**[3], and **G. Jean Harry**[1,*]

[1]Laboratory of Toxicology and Pharmacology, National Institute of Environmental Health Sciences, National Institutes of Health, Dept of Health and Human Services, Research Triangle Park, NC

[2]Department of Environmental Health Sciences, University of Alabama at Birmingham, Birmingham, AL

[3]Division of Extramural Research and Training, National Institute of Environmental Health Sciences, National Institutes of Health, Dept of Health and Human Services, Research Triangle Park, NC

Abstract

In the periphery, exercise induces interleukin (IL)-6 to downregulate tumor necrosis factor (TNF), elevate interleukin-1 receptor antagonist (IL-1RA), decreasing inflammation. Exercise also offers neuroprotection and facilitates brain repair. IL-6 production in the hippocampus following exercise suggests the potential of a similar protective role as in the periphery to down-regulate TNFα and inflammation. Using a chemical-induced model of hippocampal dentate granule cell death (trimethyltin, TMT 2.4 mg/kg, ip) dependent upon TNF receptor signaling, we demonstrate neuroprotection in mice with 2wks access to running wheel. Exercise attenuated neuronal death and diminished elevations in TNFα, TNF receptor 1, myeloid differentiation primary response gene (MyD) 88, transforming growth factor β, chemokine (C-C motif) ligand 2 (CCL2), and CCL3. Elevated mRNA levels for IL-1α, IL-1RA, occurred with injury and protection. mRNA and protein levels of IL-6 and neuronal expression of IL-6 receptor α, were elevated with injury and protection. Microarray pathway analysis supported an up-regulation of TNFα cell death signaling pathways with TMT and inhibition by exercise. IL-6 pathway recruitment occurred in both conditions. IL-6 downstream signal events differed in the level of STAT3 activation. Exercise did not increase mRNA levels of brain derived neurotrophic factor, nerve growth factor, or glial derived neurotrophic factor. In IL-6 deficient mice, exercise did not attenuate TMT-induced tremor and a diminished level of neuroprotection was observed. These data suggest a contributory role for IL-6 induced by exercise for neuroprotection in the CNS similar to that seen in the periphery.

Keywords

exercise; hippocampus; neuroinflammation; neuroprotection; interleukin-6; TNF alpha; trimethyltin

[*]corresponding author: G. Jean Harry, National Institute of Environmental Health Sciences, P.O. Box 12233, MD C1-04, Research Triangle Park, NC 27709. Ph. (919) 541-0927, Fax. (919) 541-4634, harry@niehs.nih.gov.
[#]current affiliation: Medical University of South Carolina, Charleston, SC.

1. Introduction

Key molecular and cellular players have been implicated in exercise neuroprotection for various neurodegenerative diseases and acute brain trauma/stroke (Ang and Gomez-Pinilla, 2007; Kramer and Erickson, 2007), including involvement of the innate immune system and reduction in the underlying inflammatory status. Clinical studies suggest that a reduction in brain inflammation underlies positive effects of exercise on cognitive functioning in patients suffering from neurodegenerative disease or acute brain injury (Kramer and Erickson, 2007). Additionally, down-regulation of tumor necrosis factor (TNF) signaling is associated with exercise amelioration of cognitive declines in aged and Alzheimer's disease mice (Van Praag et al, 2005; Parachikova et al., 2008; Nichol et al., 2008). In a model of ischemia/reperfusion, exercise preconditioning protects against damage in the brain via TNFα signal transduction pathway and TNF receptor (TNFR) down-regulation (Ding et al., 2006). In the amelioration of systemic inflammation by exercise a direct effect of interleukin (IL)-6 has been reported with the downregulation of TNFα and IL-1 by increasing soluble TNFR and IL-1 receptor antagonist (IL-1RA) (Tilg et al., 1994; Petersen and Pedersen, 2006).

With exercise, IL-6 is produced in muscle tissue with the depletion of glycogen (Jonsdottir et al., 2000; Colbert et al., 2001; Pedersen and Fischer, 2007). IL-6 is also produced in the brain with exercise (Nybo et al., 2002) suggesting a role for IL-6 in the downregulation of neuroinflammation and possible neuroprotection. More recent work demonstrated a selective IL-6 elevation within the hippocampus following exercise (Rasmussen et al., 2010), suggesting consideration of a similar role for localized elevation of IL-6 down-regulating TNF signaling and a diminished inflammatory-mediated response as a key role for exercise (Cotman et al., 2007). In the brain, IL-6 has both pro-inflammatory and immunosuppressive properties (Bauer et al., 2007). IL-6 production can be induced with IL-1 and neuronal depolarization (Tsakiri et al., 2008). A functional role for IL-6 in nervous system injury and repair has been demonstrated in IL-6 knockout mice with impaired peripheral nerve regeneration (Zhong et al., 1999) and conditioned injury-induced spinal axon regeneration (Cafferty et al., 2004). Constitutive over-expression of IL-6 and its soluble receptor in mice show enhanced regeneration (Hirota et al., 1996) and IL-6 transgenic mice demonstrate neuroprotection with an acute injury (Swartz et al., 2001; Penkowa et al., 2003).

Based upon the hypothesis that exercise would induce IL-6 in the hippocampus, down-regulating a local TNF response to injury thus, offering neuronal protection, we examined the impact of voluntary exercise on a model of TNF receptor activation dependent neuronal apoptosis. The prototypical neurotoxicant, trimethyltin (TMT) has been used as a model for limbic system damage. In the mouse, injury is characterized by localized dentate granule cell death with sparing of CA pyramidal cell death (Bruccoleri et al., 1998; Fiedorowicz et al., 2001; Harry et al., 2008). While the mechanism of neuronal death by TMT is not clearly determined, a causal role for TNFα has been suggested in the caspase dependent process. TMT results in the induction of TNFα production by microglia (Bruccoleri et al., 1998; Figiel and Szwonek, 2007; Harry et al., 2002; 2008), the activation of TNF receptors (Figiel and Dzwonek, 2007; Harry et al., 2008), and the ability of neutralization of TNFα signaling to diminish neuronal death (Harry et al., 2003; 2008). Using this model of selective hippocampal TNF receptor-mediated neuronal damage, we examined the neuroprotective capability of voluntary running wheel (RW) exercise, changes in mRNA levels for genes associated with IL-6 signaling, and the response in IL-6 deficient mice as they relate to the neurotoxicity.

2. Material and Methods

2.1. Animals and hippocampal injury

Pathogen-free CD-1 male mice (Charles River Labs, Raleigh, NC) were housed two per cage with littermates at weaning and maintained with housing enrichment that included Nestlett® nesting material and an igloo unit. At 120 days-of-age, mice were singularly housed using 1/3rd original bedding to minimize stress and maintained 3 days under these conditions. Randomly selected mice (matched based on the original 2/cage housing) were transferred to either a new cage with 1/3rd original bedding, Nestlett® material, and an igloo unit or placed in a new cage with 1/3rd original bedding, Nestlett® and allowed free-access to a running wheel (RW; Mini-Mitter®; Respironics Co., Bend, OR). Running wheel access was allowed for 2wks with all mice displaying a normal daily pattern of running with a total of approximately 9000 rotations within any given 24hr period. Food (NIH 31) and deionized, distilled drinking water were available *ad libitum*. All procedures complied with an approved National Institute of Environmental Health Sciences Animal Care and Use Committee protocol.

Mice from running wheel (RW) and non-running wheel (NRW) groups received an intraperitoneal (ip) injection of either saline (2 ml/kg body wt) or 2.4 mg/kg trimethyltin hydroxide (TMT) (n=40–50; 5 dosing cohorts of 8–10 mice/group) to induce a focal injury to the dentate granule neurons of the hippocampus. The injection was delivered 4hrs into the light period of a 12hr light/dark cycle (6:00–18:00). As housing conditions can influence the response of mice to insult, we confirmed that the severity and pattern of the TMT injury was not significantly influenced by conditions employed (Suppl. Fig. 1). While we did not expect a systemic toxic response with this dose level, clinically chemistry was performed on blood collected at terminal necropsy and histopathology of liver and kidney examined. Serum levels of blood urea nitrogen, glucose, alkaline phosphatase, total protein, alanine aminotransferase, creatinine, and urine pH levels were similar across dose groups and remained within normal levels. No histopathological evidence of organ damage was observed (data not shown).

Twenty-four hrs post-injection, all mice were scored during a 5-min interval on a tremor/seizure severity scale: 1=normal behavior; 2= hyperresponsiveness to sound and handling, 3= whole body mild tremor with normal motor activity; 4 = whole body tremor with extended periods of immobility; 5 = rigid posture; 6 = forelimb clonus, rearing, and falling; 7 = repeated incidence of level 4 behavior; and 8 = severe tonic-clonic behavior. Immediately following scoring, mice were euthanized, brains excised, bisected in the mid-sagittal plane. One hemisphere was immersion-fixed in 4% paraformaldehyde (PFA)/0.1M phosphate buffer (PB; pH 7.2) overnight. Brain regions were dissected from the contralateral hemisphere and either immediately frozen on dry ice for molecular analysis or homogenized in lyses buffer for protein analysis. To minimize any diurnal effects upon pro-inflammatory cytokine at time of tissue collection, all tissue was collected at 24hrs post-injection in a randomized manner across the experimental groups over a maximum time period of 1.5 hrs. All animals on study were examined histologically for severity of dentate granule cell death. Randomly selected samples across cohorts were used for the various immunohistochemical and immunofluorescent staining and molecular/biochemical analysis.

2.2. Evaluation of bone-marrow chimera mice to confirm lack of infiltrating monocytes with TMT-induced injury

To examine and confirm the level of infiltrating monocyte/macrophage contribution in the TMT model of hippocampal injury, the presence of bone-marrow derived GFP+ monocytes within the brain parenchyma was examined. Male mice, 90 days-of-age, underwent whole-

body irradiation with full head-shielding, for 110 seconds using a JL Shepherd Irradiator Model 431 (modified Mark 1) with a cesium source at ~12,000 Curies. ~9 Gray was delivered to the body and ~0.24 Gray was delivered to the hippocampus (Suppl. Material). Immediately following irradiation, 1.25×10e7 bone marrow obtained from C57BL/6-Tg(ACTB-EGFP)10sb/J (eGFP (green fluorescent protein) under chicken β-actin promoter, Jackson Labs, Bar Harbor, ME) cells were injected into the orbital sinus. Reconstitution of approximately 80% GFP+ cells was confirmed via flow cytometry of cluster of differentiation molecule (CD)11b, CD4, and GFP (Suppl. Material). This method resulted in reconstituted mice with black hair coloring on the head and grey hair coloring on the body. Following confirmed reconstitution, mice were injected with TMT and, at 72hr post-injection, brain tissues collected and processed for histology to determine presence of GFP+ cells within the hippocampus. Mice were cardiac perfused with saline followed by 4% paraformaldehyde/0.1% glutaraldehyde fixative and 10 μm cryostat sections collected. GFP + cells were localized to the subventricular zone of the lateral ventricle with no co-localization evident with ionized calcium-binding adaptor molecule 1 (Iba-1)+ microglia in the dentate granule cell layer (GCL) of the hippocampus (Suppl. Fig. 2A). Positive control samples included a direct injection of lipopolysaccharide (LPS; 4.5 EU) and interferon (IFN)γ (0.15ng) in which a number of GFP+ cells are identified within the local cortical injection site (Suppl. Fig. 2B).

2.3. Tin (Sn) analysis in brain tissue

Samples collected across 2 cohorts were randomly selected to determine the total amount of tin distributed to the brain within 24hrs of an ip administration of TMT hydroxide (2.4 mg/kg bwt). Individual samples were digested and Sn analysis was conducted using an inductively coupled plasma mass spectrometry (ICP- OES; Hewlett-Packard; Palo Alto, CA) method. This method provided a limit of detection of 0.0032 μg Sn/g and could be reliably used to determine an experimental quantitation limit of 0.025 μg Sn/g. Constitutive levels of tin were low within the control tissue; therefore, a statistical comparison was made between the two TMT dosed groups using a Student's t-test.

2.4. Tissue preparation and histological evaluation

Serial 10μm paraffin sections through the dorsal hippocampus were collected and 8 slices, at multiple planes of cut were randomly selected from each brain and stained with hematoxylin and eosin (H&E). Three observers, blind to treatment, scored cell death severity. Severity scores (0–4) were assigned for dentate granule cell death based upon number and location (progressing from the inner blade to throughout the blade of the dentate) of $eosin^+$ cells and structural characteristics of dense and collapsed chromatin. A score of 1 indicated no evidence of cell death, 2 indicated neuronal death occurring along the inner blade of the dentate to within a 3-cell layer width of the blades. A score of 3 indicated cell death throughout the entire blade of the dentate and a score of 4 indicated significant cell loss as indicated by the absence of distinct cellular material as represented by the presence of voids in the dentate granule cell layer. Using a modified-grid counting approach, the number of $eosin^+$ cells within the dentate blades was determined.

2.5. Immunohistochemistry

Sections were randomly selected across the 4 cohorts from a total of 20 mice per treatment condition and immunostained for microglia. Rehydrated sections underwent heat-induced epitope retrieval (Biocare Medical, Walnut Creek, CA) in 0.01 M citrate buffer (pH 6.0), and blocked with 10% normal goat serum/1% BSA/PBS for 30 min. Microglia were identified by staining with a rabbit polyclonal antibody to Iba-1 (1:500; 1hr, 24°C; Wako Chemicals, Richmond, VA) detected with IgG Alexafluor 488 (1:1000, Molecular Probes,

Eugene, OR) or binding of isolectin B4 (IB_4) from *Griffonia simplicifolia* (Sigma, St. Louis, MO)

To evaluate the immunoreactivity and cellular localization for IL-6 related proteins and downstream signaling molecules, sections were randomly selected across the 4 cohorts for a total of 12 mice per treatment condition and immunostained for IL-6, IL-6 receptor Rα (IL-6 Rα), gp130, phosphorylated (p)Akt, and phosphorylated signal transducer and activator of transcription 3 (pSTAT3). Endogenous peroxidase activity was blocked with 3% H_2O_2, endogenous avidin-biotin activity quenched (Vector Laboratories, Burlingame, CA) and non-specific protein binding quenched with 10% normal goat serum. Sections were incubated 18hrs at 4°C, with antibodies to IL-6 (1:500; Santa Cruz Biotechnology, Santa Cruz, CA) IL-6Rα (1:1000; Santa Cruz), gp130(1:1000, Santa Cruz), pAkt(Ser 473, 1:250), pSTAT3(Tyr 705, 1:250) developed with a Vectastain Elite ABC kit and visualized with 3,3-Diainobenzidine (DAB). IL-6 was developed with a Vectastain Elite ABC kit and visualized with a FITC-conjugated tyramide signal amplification kit. Negative controls were conducted in the absence of the primary or secondary antibody and with immuno-absorbed antibody. In many cases, the control brain sections served as a biologically negative control. Positive controls were obtained from peripheral organ tissue samples. All antibodies were tested for specificity by Western blots.

2.6. Microscopy

Digital images of fluorescent staining were acquired using a SpotRT™ camera (Diagnostic Instruments, Sterling Heights, MI) on a Leica DMRBE microscope (Wetzlar, Germany) with epifluorescence and Z-control using Metamorph™ (Universal Imaging Co., Downingtown, PA). Digital fluorescent images were captured as 16-bit monochrome images and pseudocolored. H&E and immunohistochemical images were collected at both 20x and 40x magnification using an Aperio Scanscope T2 Scanner (Aperio Technologies, Inc. Vista, CA) and viewed using Aperio Imagescope v. 6.25.0.1117.

For cell counting, a region of interest (ROI) was created for the dentate gyrus and individual eosin+ positive cells displaying characteristics of cell death and microglia were determined. The morphological phenotype of microglia were determined using a modified rating scale based upon the works of Wilms et (1997) and Heppner et al., (1998) for examining ramifications of microglia and macrophages; taking into consideration the *in vivo* sampling and the range of the cells from fine process bearing (score 1–2), to stellate process bearing (score 3–4), to amoeboid and rounded morphology (score 5–6). Given the rare occurrence of IL-6Rα and pSTAT3 staining, positive cells were counted within the entire GCL. For estimation of localized IL-6 expression in the suprapyramidal blade of the dentate gyrus, monochromatic images were thresholded and the amount of fluorescent pixels in the total ROI was determined by image segmentation and expressed as percentage of total area.

2.7. qPCR

Total RNA was isolated with TRIzol® (Gibco BRL, Gaithersburg, MD) in a manner counterbalanced across the experimental groups. Reverse transcription (RT) was performed with 2.5μg total RNA isolated with TRIzol® (Gibco BRL, Gaithersburg, MD), using SuperScript™ II Reverse Transcriptase (Invitrogen). qPCR was carried out (Perkin Elmer ABI Prism™ 7700 Sequence Detector) using 2.5μL cDNA as template, 1X Power SYBR® Green Master Mix (Applied Biosystems; Foster City, CA), and forward and reverse primers (Suppl. Table 1). 25 μl reaction mixtures were held at 50°C for 2-min, 95°C for 10-min, followed by 40 cycles at 95°C for 15-sec and 1-min at 60°C. Amplification curves from individual qPCR reactions were generated within Sequence Detection System 1.9.1.

Threshold cycle values were determined and mean fold changes over the saline/NRW group were calculated using the comparative C_T method. GAPDH was used for normalization.

2.8. Response in IL-6$^{-/-}$ mice

Pathogen free, 90-day-old male IL-6$^{-/-}$ (B6;129S2-IL6<tm1Kopf>) and wildtype B6129SF2/J (Jackson Labs, Bar Harbor, ME) mice were housed under normal conditions or with access to a running wheel as previously described. Mice received either a single intraperitoneal (ip.) injection of trimethyltin hydroxide (TMT; 2.4 mg/kg body wt) or saline in a dosing volume of 2ml/kg body wt (2 cohorts of 5 mice for total n=10). At 24hrs post-injection, mice were observed and scored for level of tremor/seizure activity. Brains were collected from mice and processed for embedding in paraffin as described earlier. Deparaffinized and ethanol rehydrated 8μm sections were stained with H&E to determine severity of hippocampal neuronal death.

2.9. Statistical Analysis

Seizure scores, H&E severity scores, and cell counts were analyzed by a 2×2 ANOVA followed by independent group mean comparisons by a Mann Whitney U for scoring and Bonferroni for cell counts. Total tin (Sn) levels in the NRW+TMT and RW+TMT group were analyzed by Student's t-test. Phagocytic scores of microglia were calculated as percentage of total microglia. For each of 3 score ranges data was analyzed by Mann Whitney U. Western blot and qPCR data were analyzed by Bartlett's test for homogeneity of variance. Data met criteria of normal distribution and were analyzed by 2×2 ANOVA. Following a significant ANOVA, Bonferroni post hoc analysis for independent group mean differences between saline and TMT within each NRW or RW group were conducted. A maximum of 5 endpoints for qPCR were assessed in any one independent group of samples and a Bonferroni correction for multiple comparisons was applied accordingly to independent group mean analysis. Comparisons were conducted between the TMT dose group and the matched saline controls, unless noted in the text. Across all tests, statistical significance was set at $p<0.05$. Any corrections due to multiple independent group comparisons resulting in failure to reach a statistical significance of $p<0.05$ is noted within the text.

2.10. Microarray Analysis

Total RNA (1μg; hippocampus pooled from 2 mice, n=3) was amplified (Affymetrix One-Cycle cDNA Synthesis Protocol). Fifteen μg of amplified biotin-cRNAs were fragmented and hybridized to Affymetrix Mouse Genome 430 2.0 GeneChip® array (Affymetrix, Santa Clara, CA) for 16hrs at 45°C using the Affymetrix Eukaryotic Target. Slides were stained with steptavidin/phycoerythrin using a double-antibody staining procedure and washed utilizing the EukGE-WS2v5 protocol of the Affymetrix Fluidics Station FS450 for antibody amplification. Arrays were scanned with an Affymetrix Scanner 3000 and data obtained using the GeneChip® Operating Software (GCOS; Version 1.2.0.037). Data were processed with an Affymetrix-specific error model for estimating measurement variance, using Rosetta Resolver, as described in Weng et. al. (2006). Biological replicates were combined through error-weighted averaging and comparison ratios were built between samples. Statistical significance was set at $p<0.001$ and a minimum fold change of 1.2 was set as criteria.

The array data examined for changes in genes related to cell death and IL-6 pathways. Probeset IDs for Biocarta pathways (http://www.biocarta.com) were downloaded using the MSigDB gene sets browser in GSEA v2.0 (http://www.broad.mit.edu/gsea/msigdb/). Biocarta pathways pertaining to cell death included: DEATH, TCAPOPTOSIS, and CASPASE. The network was generated with Ingenuity Pathways Analysis (Ingenuity System, Redwood City, CA). Each Affymetrix identifier was mapped to its corresponding

gene object in the Ingenuity Pathways Knowledge Base (Ingenuity System, Redwood City, CA). Pathways were created linking the expression of genes related to IL-6 and STAT3 signaling. A set of focus genes including, brain derived neurotrophic factor (BDNF), insulin-like growth factor-1 (IGF-1), IGF, TNF, IL-1, and IL-6 pathway members was established based on previous exercise literature. Based upon the work of Yang et al. (2007) demonstrating a STAT3 signaling pathway employing unphosphorylated STAT3 (U-STAT3) for rapid signaling events, specific target genes, MET (a receptor tyrosine kinase) proto-oncogene and muscle RAS oncogene (MRAS) were included. Rgs4, a regulator of G-protein signaling was included as a prominent gene differentially expressed ($p<0.001$) across all groups. Connections between these focus genes were developed with the Knowledge Base using the Build Pathways Connect function. Fold change in gene expression was then overlaid onto this network.

3. RESULTS

3.1. TMT-induced tremor/seizure and dentate granule cell damage attenuated by exercise

Within 24hrs post-TMT, mice, not allowed access to the running wheel, showed clinical signs of tremor and seizure activity that was attenuated by RW access (Fig. 1). Using a seizure severity scale as described in Methods, significant main effects of TMT [$F=66.88$ 1,164; $p<0.0001$] and RW [$F=59.52$ 1,164; $p<0.0001$] and TMT x RW interaction [$F=54.86$ 1,164; $p<0.0001$] were indicated. In NRW+TMT mice, the seizure score was significantly elevated over controls [$t=26.56$; $p<0.0001$]. Mice allowed 2wks of exercise prior to TMT did not exhibit seizures and scores were not significantly different from those recorded in RW mice dosed with saline [$t=1.31$; $p>0.05$].

Consistent with previous reports, the neuropathology of the acute TMT injection was characterized by death of dentate granule neurons in the hippocampus (Fig. 2A). This was accompanied by a microglia response to the local neuronal insult (Fig. 2C). Consistent with the published neuropathology induced by this compound in mice, there was no evidence of damage to the pyramidal neurons. H&E stained neurons throughout the blades of the dentate gyrus displayed a cytoplasmic presence of eosin and collapsed and coalesced morphology (Fig. 2A, arrows). Using a histopathology severity scale described in Methods, a significant main effect of TMT [$F=275.7_{1,164}$; $p<0.0001$], RW [$F=232.6_{1,164}$; $p<0.0001$] and significant TMT x RW interaction [$F=212.4_{1,164}$; $p<0.0001$] were noted. The significant neuronal death observed in NRW + TMT mice [$t=22.05$; $p<0.0001$] was not observed in the mice allowed access to the RW [$t=1.43$; $p>0.05$] (Fig. 2B). To assess whether this represented a blockage of neuronal death or a delay, 10 mice randomly assigned across the TMT cohorts were examined for histopathology at 72hrs post-TMT. The H&E staining pattern was similar to that observed at the 24hr time point with no evidence of eosin+ neurons in the dentate granule cell layer (Fig. 2A). Quantitation of the number of eosin+ cells within a defined ROI as described in Methods indicated significant main effects of TMT [$F=1011_{1,96}$; $p<0.0001$], RW [$F=997.9_{1,96}$; $p<0.0001$] and TMT+RW interaction [$F=949.8_{1,96}$; $p<0.0001$] by a 2×2 ANOVA. NRW + TMT mice demonstrated an increase in the estimated number of eosin+ neurons showing collapsed and coalesced morphology [$t=44.27$; $p<0.0001$] as compared to controls (Fig. 2B). Consistent with the representative image (Fig. 2A), no difference was observed for cell death across the 3 remaining groups.

The microglia response was similar to what has been previously described for this model (Bruccoleri et al., 1998; Harry et al., 2008). In the normal brain, microglia display few cell bodies within the GCL however, there was evidence of fine processes throughout the area (Fig. 2C). With injury induced by TMT, microglia showed a shift in morphology and at 24hrs, the cells displayed thickened processes with stellate morphology throughout the GCL (Fig. 2C). With exercise, microglia within the GCL displayed thickened and less complex

process (Fig. 2C). In the absence of neuronal death occurring in RW+TMT mice, the morphological phenotype of microglia was different than observed in other groups with cells showing a more oval cell body structure and less process arborization and a primary localization along the SGZ (arrow, 2C). In the absence of exercise, TMT dosing resulted in an increase in the number of $Iba1^+$ microglia observed within the GCL that was significantly greater than the elevation seen in TMT dosed mice allowed RW access [$t=9.11_{22}$; $p<0.0001$) (Fig. 2D). Quantitative estimates of the morphological response were conducted using a rating scale for the process bearing to stellate and amoeboid morphology as described in Methods. In sedentary mice dosed with TMT, the injury response of microglia showed a primary distribution of cells showing a stellate morphology (Score 3–4). In comparison, mice allowed access to the RW prior to dosing with TMT (RW+TMT) showed a different microglial morphological phenotype with a greater percentage of total microglia falling within the range of 1–2 ($p<0.0001$) and 5–6 ($p<0.0001$) with significantly less percentage seen within the score range of 3–4($p<0.0001$) primarily observed in the sedentary TMT dosed mice (Fig. 2D). The changes in microglia in the absence of neuronal death may likely be associated with the proliferative induction of new cells in the SGZ with exercise and with TMT. While a full interpretation of the nature of the microglia response seen in the RW mice cannot be determined by the current data set, there is clearly a significant difference in the microglia response to the injury induced by TMT as a function of exercise. To gain a better understanding of the morphological phenotype observed at 24hrs, we examined the progression of the microglia response at 72hrs post-TMT (Fig. 2E,F). In the NRW+TMT mice, a clear amoeboid phagocytic morphology of IB4+ microglia (Score was evident throughout the dentate granule cell blades in sedentary mice. In the RW+TMT mice a process bearing microglia response remained with little indication of amoeboid microglia.

3.2. Sn concentration

To determine if the absence of hippocampal damage observed with RW was associated with lower level of the compound reaching the brain, Sn concentrations were determined at 24hrs. In the saline control groups, both NRW and RW, a signal for Sn was just barely detected and concentrations were under the quantitation limit thus, could only be estimated as 0.01 μg Sn/g tissue. Twenty-four hours following the injection of TMT, Sn concentrations were significantly elevated above the quantitation limit. Sn concentrations in mice allowed free access to the running wheel for 2wks prior to an injection of TMT (RW = 2.0 ± 0.3ug Sn/g tissue) were similar to those obtained in mice that were maintained in a normal home cage prior to TMT injection (NRW = 2.2 ± 0.4ug Sn/g tissue).

3.3. Elevations in IL-6 with TMT and with RW+TMT

At 24hrs following the TMT injection, mRNA levels for IL-6 were elevated in the hippocampus in sedentary mice and mice allowed 2wks access to RW (Fig. 3A). This was observed in three independent analyses (n=6 each) across the course of the study. Statistical analyses conducted by a 2×2 ANOVA indicated a significant main effect of treatment [$F=15.46_{\mathbf{1,20}}$; $p<0.0008$; $F=24.29_{\mathbf{1,20}}$; $p<0.0001$; $F=22.4_{\mathbf{1,20}}$; $p<0.0002$] in each cohort, respectively. No significant main effects of RW [$F=2.01_{\mathbf{1,20}}$, $p<0.17$; $p<0.097$; $p<0.16$] or TMT x RW interaction [$F=0.0044_{\mathbf{1,20}}$; $p<0.95$; $p<0.96$; $p<0.97$] were detected. Bonferroni post-hoc analysis indicated a significant elevation in IL-6 mRNA levels in NRW mice injected with TMT ($t=16.2$ to 18.3; $p<0.0001$) and in RW mice injected with TMT ($t=15.9$ to 18.8; $p<0.0001$).

TMT exposure increased IL-6 protein expression within the GCL (Fig. 3B). When we examined the localized expression for IL-6 protein within the dentate granule cell layer, saline dosed mice displayed immunoreactivity that was localized within blood vessels along the vascular wall (Fig. 6B). No immunoreactivity was observed within the brain

parenchyma. Twenty-four hours following the TMT injection, the immunoreactive product for IL-6 was increased and diffusely distributed in a fibrous-type pattern throughout the dentate granule cell layer and was not detected within DAPI+ neurons (Fig. 3B). Estimates of protein level within the GCL by fluorescent pixel assessment indicated a significant increased [$F=299.5_{1,24}$; $p<0.0001$] expression with TMT in both the NRW [$t=15.13$; $p<0.0001$] and RW [$t=9.35$; $p<0.0001$] conditions as compared to controls (Fig. 3C). Efforts to co-localize IL-6 suggested no localization to neurons and localization to GFAP+ astrocytes (Suppl. Fig. 3).

We then examined the expression pattern for the two IL-6 receptors, IL-6Rα and gp130. In control tissue, immunostaining for IL-6Rα showed a slight reactive product around individual dentate granule neurons with no indication of intracellular staining (Fig. 4A). This pattern was not altered with exercise. Within 24hrs following an injection of TMT, IL-6Rα immunoreactive product was detected in dentate granule neurons both in cells displaying normal morphology and those showing a collapsed and condensed morphology. In RW+TMT mice, IL-6Rα was expressed in neurons showing normal morphology scattered throughout the GCL.

The IL-6/IL-6R complex initiates signaling through the gp130 receptor to regulate cell growth, proliferation, differentiation, and apoptosis. gp130 immunoreactive product was detected in the cytoplasm and radiating processes of cells within the GCL (Fig. 4B). An increased immunoreactive product was observed within the cytoplasm of collapsed neurons in the NRW+TMT group. Individual punctate areas of dense staining and staining within neuronal nucleus were occasionally evident in the RW+TMT group. IL-6Rα/gp130 activation initiates STAT3/Akt signaling. In saline control mice, pSTAT3 immunoreactivity (Fig. 4C) was not detected in the GCL. In the NRW+TMT mice, pSTAT3 immunoreactive product was detected in the nucleus of intact dentate granule neurons as well as in neurons showing a condensed and collapsed morphology (Fig. 4C). In the RW+TMT group, immunostaining for pSTAT3 was localized to only a few individual neurons suggesting that activation of the pSTAT3 pathway was limited under neuroprotective conditions. As pSTAT3 signals via pAKT, we examined pAKT immunostaining in the GCL and identified staining only with interneurons within the hilus with TMT and no staining was observed within the GCL (data not shown). For IL-6Rα estimate of the number of immuopositive cells showed a significant main effect of TMT by 2×2 ANOVA [$F=5784_{1,20}$; $p<0.0001$]. Bonferroni multiple comparisons showed significant elevations in number of neurons expressing IL6Rα in NRW+TMT [$t=53.81$; $p<0.0001$] and RW+TMT [$t=53.74$; $p<0.0001$] relative to controls (Fig. 4D). For pSTAT3, an estimate of the number of immunopositive cells showed significant main effects of TMT by a 2×2 ANOVA [$F=779.5_{1,20}$; $p<0.0001$], RW [$F=210.8_{1,20}$i;$p<0.0001$] and a significant TMT x RW interaction [$F=210.8_{1,20}$;$p<0.0001$]. Bonferroni multiple comparisons showed significant elevations in number of neurons expressing pSTAT3 in NRW+TMT [$t=30.01$; $p<0.0001$] and RW+TMT [$t=56$; $p<0.0001$] relative to controls and a significant higher number of cells in the NRW +TMT group as compared to the RW+TMT group [$t=12.65$; $p<0.0036$) (Fig. 4E). The immunoreactivity staining pattern for gp130 was not localized in a manner conducive for cell counting but the was sufficient to detect protein by Western blots and no increases were detected in protein level over the experimental conditions (Fig. 4E).

3.4. qPCR for genes elevated with TMT-induced neuronal death

Injury to dentate granule neurons by TMT is accompanied by an elevation in mRNA levels of genes associated with neuroinflammation. A 2wk access to the RW prior to the TMT injection blocked these elevations suggesting an inhibition of the localized neuroinflammatory response. This pattern was evident for chemokine (C-C motif) ligand 2 (CCL2), CCL3, TNFα, TNFR1, and IL-1.

CCL-2 and CCL-3—mRNA levels for the chemokine, CCL-2 (also known as monocyte chemotaxic protein-1 (MCP-1)) showed a statistically significant increase with TMT [F=14.83; df=$_{1,20}$; p=0.001], RW [F=4.99, df=$_{1,20}$; p=0.037] and TMT x RW interaction [F=4.38; df=$_{1,20}$; p<0.049]. Bonferroni post-hoc analysis indicated a significant increase in CCL-2 in sedentary mice exposed to TMT [p<0.001] (Fig. 5A). mRNA levels for the chemokine, CCL-3 (also know as macrophage inflammatory proteins (MIP-1α)) were significantly increased with TMT [F=20.59; df=$_{1,20}$; p=0.0002] with no main effect of RW [p=0.086] or TMT x RW interaction [p=0.084]. Bonferroni post hoc analysis indicated a significant increase in CCL-3 mRNA levels in sedentary mice injected with TMT [t=4.49; p<0.001]. mRNA levels were elevated in the RW mice injected with TMT however, this failed to reach statistically significance [t=1.92; p>0.05] as compared to RW saline mice (Fig. 5B).

TNFα and receptors—In agreement with earlier work on the TMT model from our lab and others, within 24hrs post-TMT, mRNA levels for TNFα and TNFR1 were significantly elevated with injury. This elevation was attenuated with exercise. Levels for TNFα showed a significant main effect of TMT [F= 168 $_{1,44}$; p<0.0001], RW [F=149.8$_{1,44}$; p<0.0001] and a significant TMT x RW interaction [F=150.8$_{\mathbf{1,44}}$; p<0.0001]. Bonferroni multiple comparisons indicated a significantly higher mRNA level of TNFα in the NRW+TMT group [t=17.85; p<0.0001] (Fig. 6). For TNFR1 a significant main effect of TMT [F=30$_{\mathbf{1,20}}$; p<0.0001], RW [F=20.59$_{\mathbf{1,20}}$;; p=0.0002] and a significant TMT x RW interaction [F=5.946$_{\mathbf{1,20}}$; p=0.242] were detected. Bonferroni post hoc tests indicated a significant increase in TNFR1 in sedentary mice injected with TMT [t=5.60; p<0.001] (Fig. 6). For TNFR2, a significant main effect of TMT [F=8.18$_{\mathbf{1,20}}$; p=0.0097] was detected with no significant main effects of RW [F=6.44$_{\mathbf{1,20}}$; p=0.20] or TMT x RW interaction [F=0.25;p=0.62] (Fig. 6). One mechanism by which IL-6 can regulate TNFα is by increasing soluble TNFR1 (Petersen and Pedersen, 2006); however, as examined by Western blots, TNFR1 protein levels in the entire hippocampus were similar across all groups (Suppl. Fig. 4) but sub-dissected GCL regions were not examined.

IL-1, IL-1R, IL-1RA, and myeloid differentiation primary response gene (MyD88)—No significant main effects or interaction were detected for IL-1β and IL-1R (Fig. 7). A 2×2 ANOVA for IL-1α determined a significant main effect of TMT [F=18.36 1,44; p<0.0001] with no main effect of RW or significant interaction. Bonferroni post hoc test indicated a significant increase (t=3.074; p<0.01) in IL-1α mRNA levels in the NRW +TMT mice (Fig. 7). IL-6 can regulate IL-1 by increasing IL-1RA (Tilg et al., 1994; Petersen and Pedersen, 2006). mRNA levels for IL-1RA showed a significant main effect of TMT [F=30.49$_{\mathbf{1,20}}$; p<0.0001], RW [F=9.99$_{\mathbf{1,20}}$; p=0.0049], and TMT x RW interaction [F=10.12$_{\mathbf{1,20}}$; p=0.0047]. Bonferroni post-hoc test indicated significantly higher levels in NRW+TMT [t=6.15; p<0.001] and RW+TMT mice [t=2.34; p<0.05] as compared to relative saline controls (Fig. 7). MyD88 is recruited to the IL-1α/IL-R1 complex to activate the IL-1 receptor associated kinase (Wesche et al., 1997). Analysis of mRNA levels for MyD88 showed a significant main effect of TMT [F=31.73$_{\mathbf{1,20}}$; p<0.0001], RW [F=7.38$_{\mathbf{1,20}}$; p=0.013] and TMT x RW interaction [F=8.47$_{\mathbf{1,20}}$; p=0.0087]. Bonferroni post hoc analysis indicated a significant elevation only in the NRW+TMT mice [t=6.04; p<0.001] (Fig. 7).

3.6. qPCR for anti-inflammatory and neurotrophic related genes

Alternative mechanisms of neuroprotection were examined by qPCR of genes that have been associated with exercise, transforming growth factor beta (TGFβ), glial derived neurotrophic factor (GDNF), BDNF, and nerve growth factor (NGF) (Fig. 8). The only elevations observed were with injury, suggesting the induction of an anti-inflammatory process to down regulate the inflammatory environment. The absence of an inflammatory

response in the RW+TMT group did not induce an elevation of mRNA levels for these genes. As indicated by a 2×2 ANOVA, a significant main effect of TMT [$F=13.8_{\mathbf{1,20}}$; p=0.0014] and TMT x RW interaction [$F=5.5_{\mathbf{1,20}}$; p=0.29] were detected for TGFβ mRNA levels. Bonferroni post hoc analysis confirmed a significant elevation in the NRW+TMT group [t=4.29; p<0.001] as compared to controls. A significant main effect of TMT [$F=34.07_{\mathbf{1,20}}$; p<0.0001] was observed for IGF-1 with no significant main effect of RW [p=9.06] or TMT+RW interaction [p=0.48]. NRW+TMT mice displayed an elevated mRNA level of IGF-1 as compared to controls [t=4.6;p<0.001]. Under each of the experimental conditions, mRNA levels for BDNF, GDNF, and NGF remained within control levels and were not found to be elevated with either TMT or the limited 2wk access to the RW.

3.7. Diminished Neuroprotection in IL-6$^{-/-}$ mice

To examine the contributory role of IL-6 in the attenuated injury response with RW, we examined the response in IL-6$^{-/-}$ mice. Data is collapsed across two individual cohorts of mice. In B6129SF2/J (WT) mice, TMT produced a similar tremor/seizure response as CD-1 mice and an absence of clinical signs was observed when the mice were allowed access to the RW. In IL-6$^{-/-}$ mice, no clinical evidence of neuroprotection from RW access was observed and all mice displayed significant whole body tremor. Significant main effects of RW [$F=66.46_{1,36}$; p<0.0001], genotype [$F=55.85_{1,36}$;p<0.0001] and RW x genotype interaction [$F=16.62_{1,36}$; p<0.0002] were indicated by a 2×2 ANOVA. Wildtype mice showed a significant attenuation of the tremor/seizure response [Mann Whitney U = 1; p<0.0001] that was not observed in the IL6$^{-/-}$ mice (Fig. 9A). TMT produced a similar pattern of hippocampal damage in both WT and IL-6$^{-/-}$ sedentary mice, with death of dentate granule neurons. With exercise, both WT and IL-6$^{-/-}$ mice showed a lower level of neuronal death following TMT (Fig. 9B, C). A significant main effect of exercise [$F=136_{1,28}$;p<0.0001], genotype [$F=36.69_{1,28}$;p<0.0001], and exercise x genotype interaction [$F=31.55_{1,28}$; p<0.0001] was detected for severity of neuronal death. For the number of eosin^{+} cells, significant main effects of exercise [$F=265.3._{1,28}$;p<0.0001), genotype [$F=36.69_{1,28}$; p<0.0001] and exercise x genotype interaction [$F=47.27_{,1,28}$;p<0.0001]. Boneferroni multiple comparisons indicated a significant decrease in WT mice allowed to exercise prior to TMT [t=15.8, p<0.0001] as well as in IL-6$^{-/-}$ mice [t=7.25;p<0.0001]; however, the change in cell death as a function of exercise was significantly less in the IL-6−/− mice as compared to WT [t=10.2; p<0.0001].

3.8. Microarray Analysis

With exercise alone, a limited number of genes reached the strict criteria of statistical significance of p<0.001 and ≥ 1.2 fold change in expression (Suppl. Table 2). The prominent increased transcripts included, metallothionein 1K (MT2A), an antioxidant, zinc binding protein induced by IL-6 (Lee et al., 1999), insulin-like growth factor binding protein 6 (Igfbp6), and growth hormone releasing hormone (Ghrh), an inducible factor for hippocampal progenitor cells. The pre-proenkephalin 1 gene, Penk1, a regulator of a stress response was elevated, as were dystrobrevin-α (Dbx2), the G-protein, Rgs4 transcript, and a basic transcription element binding protein, Klf9.

With regard to down-regulated genes with exercise (Suppl. Table 2), a number were related to metabolism and glucose utilization, including glyoxalase 1 (Glo1), a protein expressed in dentate granule neurons and Fatso (Fto), also expressed in hippocampal neurons. A prominent down-regulation was seen for GLP-1R, the receptor for glucagon-like peptide-1 (GLP-1) that regulates glucose homeostasis and activates adenylate cyclase in the brain. A decrease was seen in Cdc42ep2, a member of the Rho GTPase family that regulates multiple cellular activities. Decreases were seen in the heat shock protein, Hspa8, and in neuronal PAS domain protein 4 (Npas4), a gene expressed in the limbic system and differentially

expressed in ischemia. Significant decreases were seen for the neural stem cell marker, Sox2, and Fanconi anemia complementation group C (Fancc); both impact growth and survival of progenitor cells.

The overall general patterns of neuronal injury and protection observed by histopathology and qPCR were supported by the molecular profiles generated from the microarray analysis. Significant changes in genes associated with Biocarta pathways pertaining to cell death were seen in the hippocampus of mice injected with TMT (Table 1). In the Non-Running Wheel +TMT mice, significant elevations were seen in caspase 3 and in the caspase 8 and FADD-like inhibitory protein, FLIP, that can inhibit both TNFR and Fas cell death signaling (Micheau et al., 2001). This elevation may reflect an active effort to impede TNFα-induced apoptosis by inhibiting TNFR activation (Taoufik et al., 2007). Inhibitor of nuclear factor kappa-B kinase subunit alpha (IKKα) was elevated which can occur in response to signaling via a specific subset of TNF family members (Hacker and Karin, 2006) and serves to regulate the nuclear factor kappa-light-chain-enhancer of activated B cells (NF-κB; Karin and Ben-Neriah, 2000). Elevations were seen in the nuclear factor of kappa light polypeptide gene enhancer in B cells inhibitor alpha (NFκBIA), which blocks nuclear translocation of NF-κB DNA binding and phosphorylation by protein kinase alpha (Ito et al., 1995). A slight elevation was seen in the p65 RelA subunit that contributes to TNFα signaling as demonstrated that mice deficient for RelA/p65 die due to an uncontrolled TNFα-mediated apoptosis (Beg et al., 1995). The gene changes in the Biocarta cell death pathways seen with TMT were attenuated with prior exercise and transcript levels remained within control range, consistent with histological evidence of neuroprotection (Table 1,2).

With both TMT and Running Wheel+TMT, elevations were seen by microarray in the Biocarta IL-6 pathway (Table 3). IL-6 binds to the IL-6 receptor-α (IL-6Rα), then to the gp130 receptor to initiate signal transduction via the Janus tyrosine kinase /STAT3 (JAK/STAT3) and phosphatidylinositol (PI)-3 kinase/Akt pathways. These pathways can be employed for cell survival (Reich, 2007). As an alternative to the pSTAT3/pAKT pathway, IL-6 acts through multiple downstream effectors including the small monomeric G protein, Ras (RAt Sarcoma) for protection of myeloma cells from apoptosis (Rowley and van Ness, 2002). Hras1 (H-ras. Harvey) was elevated with TMT-induced injury and blocked by previous exercise. Fos mRNA levels were not elevated with exercise or TMT alone but were significantly elevated with neuroprotection in the Running Wheel+TMT group (Table 2).

Focused Network Analysis for comparisons between injury and neuroprotection—Next, we sought to analyze our genome wide expression results in the context of previous literature for exercise. Ingenuity Pathways Analysis was used to build a network connecting these genes with genes in the IL-1 and IL-6 pathways (Fig. 10). pSTAT3 is normally considered the activated form of the protein to drive inducible gene expression. However, a capacity for the unphosphorylated form of STAT3 (U-STAT3) to drive transcription of many genes involved in oncogenesis, cell cycle control, and the immune response has been demonstrated (Yang et al., 2005). Thus, we expanded the network to connect the downstream targets of the IL-6/U-STAT3 pathway. These pathway specific genes include the transmembrane tyrosine kinase, MET, a member of the Fas family of small GTPases, MRAS, and the Th1 related chemokine, CCL5 (Yang et al. 2007). In addition, we observed that the transcript for the G protein, Rgs4, was differentially expressed ($p<0.001$) across all groups and was included in this analysis. Network comparisons were made between control mice and mice exposed to (A) RW, (B) NRW +TMT, or (C) RW+TMT. The IL-1β and IL-6 pathways were up-regulated in injury (TMT; Fig. 10A) and neuroprotection (RW+TMT; Fig. 10C). mRNA levels for the proto-ongogene, MET, the Ras-related protein, MRAS, and CCL5 were elevated with exercise but were not induced with injury (Fig. 10B). In the hippocampus of mice allowed access to the RW prior

to the TMT injection, the expression pattern varied. CCL5 levels were elevated similar to that seen with RW alone; however, the induction of MET and MRAS observed with exercise was not evident when mice received TMT (Fig. 10C).

4. Discussion

The ability of physical exercise to modify the brain environment in such a way that neurons are protected from rather severe insults provides an opportunity to unmask endogenous neuroprotective factors/actions. We demonstrate that physical exercise can offer significant protection to the hippocampus in a chemical-induced injury model that involves TNF receptor signaling. In sedentary mice, a systemic injection of TMT produced selective loss of dentate granule neurons within 24hrs and was accompanied by activation of microglia and elevations in mRNA levels for pro-inflammatory cytokines and receptors, as well as, IL-6, IL-1RA, and TGFβ as potential anti-inflammatory factors. Mice allowed a 2wk access to a RW prior to the TMT injection, a full attenuation of the damage response was observed. This was also accompanied by a significant elevation in both IL-6 and IL-1RA mRNA levels and repressed elevations of chemokines and pro-inflammatory cytokines. We further demonstrated a functional role for IL-6 in this neuroprotection in mice deficient for IL-6 by the continued manifestation of clinical signs with TMT regardless of exercise conditions and a modification of the injury response.

The hypothesis that IL-6 contributes to neuroprotection from exercise is based largely on regulation of TNFα and the role TNF receptor activation in dentate granule cell death. TNFα signaling from microglia has been proposed as a causative factor in dentate granule cell death following TMT (Eskes et al., 2003; Harry et al., 2002; 2008), possibly in conjunction with the highly-conserved growth regulating peptide, stannin (Snn) (Billingsley et al., 2006), which can be induced by TNFα (Reese et al., 2006) and is expressed in neurons vulnerable to TMT (Toggas et al., 1992). Previously, we identified a requirement of activation and internalization of TNF receptors leading to apoptosis with TMT (Harry et al., 2008). A role for IL-6 within this injury was demonstrated by the exacerbation of TMT-induced neuronal apoptosis with *in vivo* neutralization of IL-6 (Harry et al., 2003). In addition, the neutralization of IL-6 was sufficient to mitigate the protective effects seen with TNFα neutralization suggesting a role for IL-6 in regulating injury-induced TNFα responses (Harry et al., 2003). A primary beneficial role for exercise-induced IL-6 in the periphery is related to the downregulation of TNFα. In human subjects, IL-6 is elevated within the blood following physical activity and actively blocks TNFα signaling. Initial work by Starkie et al. (2003) demonstrated that 3hrs of cycling was sufficient to blunt the normal 2–3 fold increase in circulating levels of TNFα induced by endotoxin and that this beneficial effect was mimicked by the infusion of IL-6. A regulatory role for IL-6 on TNFα levels in the periphery was further demonstrated in anti-IL-6-treated mice and in IL-$6^{-/-}$ mice (Matthys et al., 1995; Mizuhara et al., 1994). While the primary source of circulating IL-6 with exercise is muscle, Nybo et al., (2002) reported a 5-fold elevation in the release of IL-6 from the brain into the circulating blood with repeated 60-min bouts of exercise. More recently, an examination of multiple brain regions indicated elevated IL-6 mRNA levels selectively in the hippocampus following exercise (Rasmussen et al., 2010). A role for exercise and the downregulation of TNFα in the brain has been suggested by numerous studies. In a model of post-ischemic recovery, the beneficial effects of exercise on neurons within the ischemic prenumbra have been associated with a down regulation of TNF receptor signaling (Ding et al., 2006). In a more chronic degenerative model using an Alzheimer's disease transgenic mouse, Nichol et al. (2008) demonstrated that exercise-enhanced cognitive performance was associated with a downregulation of TNFα in the brain. The actual mechanism by which exercise downregulates TNFα in the brain has not been previously examined however, the neuroprotective effects of exercise on TNFα-mediated events, the local induction of IL-6

with exercise, and the down-regulation of TNFα inflammation by IL-6 strongly suggest a modulatory contribution of IL-6.

Binding of IL-6Rα to gp130 receptor leads to further signaling through the activation of STAT3 (Nakajima et al., 1996; Bromberg and Darnell, 2000). Constitutive protein expression for pSTAT3 in the GCL was not detected by immunohistochemistry; however, under both injury and neuroprotection conditions a distinct immunoreactive product was observed within dentate granule neurons. This expression level was different between the two groups in that the sedentary TMT mice showed significant elevation in the number of neurons expressing pSTAT3, while with exercise, a much lower level of staining was observed. STAT3 is activated by cytokine and growth factor binding to cell surface receptors (Darnell et al., 1994; Ihle, 1996). Thus, the differential expression level of pSTAT3 between the two TMT groups is likely related to the local levels of cytokines and growth factors, each being higher with injury. pSTAT3 activates transcription for multiple cellular functions including proliferation, anti-apoptosis, cellular transformation, differentiation and apoptosis (Chapman et al., 1999). Additionally, unphosphorylated STAT3 maintains signaling properties driving transcription of many genes, including those important in oncogenesis, cell cycle control, and immune responses (Yang et al., 2005). Using cells modified to prevent the phosphorylation of STAT3, Yang et al (2007) demonstrated that both forms of STAT3 can drive the expression of genes, such as MET, MTAS, and CCL5 and that unphosphorylated STAT3 drives a rapid and higher level of expression through its ability to interact with unphosphorylated NF-κB. Thus, the lower level of pSTAT3 staining observed in the RW+TMT mice may not necessarily indicate lower signaling but rather differential signaling suggesting that IL-6 can serve in a dual manner. With a classic injury response, elevated IL-6, combined with inflammation and multiple cell injury signals, activates STAT3 for multiple signaling events including both cell death and cell survival. In the absence of other pro-inflammatory cytokines and growth factors, elevated IL-6 may recruit the unphosphorylated STAT3 pathway for regulating cellular events or work through non-transcriptional processes to rapidly block TNFα signaling and prevent neuronal death. In support of a role for STAT3 in neuronal response to injury, a transient expression of total STAT3 in the absence of pSTAT3 has been previously reported in septo-hippocampal projection neurons within one day of an entorhinal cortex lesion (Xia et al.; 2002). Schubert et al. (2005) also reported a transient STAT3 expression in axotomized medial septal neurons with a transient expression observed at 3–4 days post-injury. Further understanding of the signaling pathways of STAT3 may aid characterization of IL-6 the early stages of neuroprotection.

While we propose that the mechanism by which IL-6 offers neuroprotection in the TMT model is via the downregulation of TNFα signaling, an alternative and likely component to the effect is the downregulation of oxidation stress responses. Oxidative stress has been proposed as one mechanism of neuronal death following TMT (Geloso et al., 2002) and an induction of oxidative stress response can augment TMT-induced neuronal injury (Yoneyama et al., 2008). However, questions remain as to whether oxidative stress is a causative factor in the initiation or a secondary process occurring with neuronal death. The regulatory role for IL-6 on the oxidative stress response and neuroinflammation appears complex and dependent upon the microenvironment. Lee et al (1999) demonstrated that the antioxidant proteins, metalothionein I and II can be induced by IL-6. A functional role for this induction was demonstrated in IL-6 transgenic mice and the ability of these anti-oxidant proteins to protect against the neuropathology that develops with age (Molinero et al., 2003). While we did not examine biochemical markers for cellular defenses against oxidative stress, we did examine data generated in the microarray profile and found that metalothionein 2A (MT2A) mRNA levels were increased with exercise alone (5.37 fold change as compared to sedentary mice; p=2.90E-04). This observation presents the

possibility that neuroprotection and promotion of recovery following injury, often reported with exercise, can be related to the promotion of anti-oxidative properties. Whether this is a primary role in the TMT model is not clear given that the microarray profile did not indicate a differential elevation of genes related to oxidative stress with TMT or with exercise neuroprotection. A role for IL-6 in regulating oxidative stress and neurodegeneration has been suggested in the studies of Penkowa et al (2000) where they reported elevated responses in mice deficient for IL-6. However, these mice also displayed an impaired inflammatory response that may have contributed to cell death. In the current study, we examined the neuroprotective capabilities of exercise in the IL-$6^{-/-}$ mice. In WT mice, exercise fully abated clinical signs of tremor induced by TMT as well as neuropathology. This protection was not observed in mice deficient for IL-6 and the mice displayed tremors following TMT regardless of exercise condition. Given the shift in response to injury previously reported for the IL-$6^{-/-}$ mice (Penkowa et al., 2000), it was not unexpected that, for neuropathology, we did not observe a complete loss of exercise neuroprotection against TMT but rather a partial response. Within the limitations of the IL-$6^{-/-}$ mouse data, the diminished protection with exercise raises questions with regard to other possible physiological changes occurring with exercise that could influence the neuropathology from TMT. Modulatory effects on the hypothalamic-pituitary-adrenal (HPA) axis have been suggested for voluntary wheel exercise. These effects appear to be dependent upon the level of the stressor and the length of time for exercise (Campeau et al, 2010; Droste et al., 2007; Joels, 2007). These studies demonstrated an increased vulnerability of dentate granule neurons with mild stressors requiring an exercise period of longer than 3 wks. The involvement of corticosteroids in TMT-induced neuropathology remains in question; however, the selective nature of the damage to the dentate granule neurons both with TMT and with adrenalectomy, continues to raise this possibility. Shuto et al (2009) reported a 2-fold elevation of plasma corticosterone levels at 2 days following TMT and an increase vulnerability to TMT with the additional insult of adrenalectomy. The work of Morita et al. (2006) suggested that TMT-induced elevation in plasma corticosterone is dependent upon expression of neuropeptide adenylate cyclase-activating polypeptide (PACAP) yet, the inhibition of plasma corticosterone in mice deficient for PACAP did not block the tremor induced by TMT. These studies suggest that changes in the HPA axis response would not be a contributing factor to the neuroprotection observed in the current study.

A significant body of literature exists demonstrating an elevation of IL-6 with exercise in addition to the biological effects of such elevation on the down-regulation of pro-inflammatory cytokines and inflammation. While numerous studies have suggested that neurotrophic factors such as BDNF are contributory to the effects of exercise on the brain and the response to injury and repair, we now demonstrate that protection offered by exercise in preventing neuronal death involves IL-6. The critical role of TNF receptor signaling in determining the death of dentate granule neurons following a systemic injection of TMT suggests that IL-6 is providing neuroprotection via a similar mechanism as demonstrated in the periphery. The TMT injury model offers the ability to identify critical factors delineating the contributory roles of IL-6 involved in neuroprotection and to identify interactions with other neuroprotective modulatory factors.

Supplementary Material

Refer to Web version on PubMed Central for supplementary material.

Acknowledgments

The authors thank the NIEHS Microarray Core for their expert assistant with the microarray analysis and Dr. Sue Edelstein for graphics support. This study was supported by the Division of Intramural Research, NIEHS/NIH under project #1Z01ES101623 and contract #N01-ES-65554, Research Triangle Institute, RTP, NC.

References

Ang ET, Gomez-Pinilla F. Potential therapeutic effects of exercise to the brain. Curr Med Chem. 2007; 14:2564–2571. [PubMed: 17979709]

Bauer S, Kerr BJ, Patterson PH. The neuropoietic cytokine family in development, plasticity, disease and injury. Nat Rev Neurosci. 2007; 8:221–232. [PubMed: 17311007]

Beg AA, Sha WC, Bronson RT, Ghosh S, Baltimore D. Embryonic lethality and liver degeneration in mice lacking the RelA component of NF-κB. Nature. 1995; 376:167–170. [PubMed: 7603567]

Billingsley ML, Yun J, Reese BE, Davidson CE, Buck-Koehntop BA, Veglia G. Functional and structural properties of stannin: roles in cellular growth, selective toxicity, and mitochondrial responses to injury. J Cell Biochem. 2006; 98:243–250. [PubMed: 16453279]

Bromberg J, Darnell JEJ. The role of STATs in transcriptional control and their impact on cellular function. Oncogene. 2000; 19:2468–2473. [PubMed: 10851045]

Bruccoleri A, Brown H, Harry GJ. Cellular localization and temporal elevation of tumor necrosis factor-alpha, interleukin-1alpha, and transforming growth factor-beta mRNA in hippocampal injury response induced by trimethyltin. J Neurochem. 1998; 71:1577–1587. [PubMed: 9751191]

Cafferty WBJ, Gardiner NJ, Das P, Qiu J, McMahon SB, Thompson SWN. Conditioning injury-induced spinal axon regeneration fails in interleukin-6 knock-out mice. J Neurosci. 2004; 24:4432–4443. [PubMed: 15128857]

Campeau S, Nyhuis TJ, Sasse SK, Kryskow EM, Herlihy L, Masini CV, Babb JA, Greenwood BN, Fleshner M, Day HEW. Hypothalamic pituitary adrenal axis responses to low-intensity stressors are reduced after voluntary wheel running in rats. J Neuroendocrinol. 2010; 22:872–888. [PubMed: 20406350]

Chapman RS, Lourenco PC, Tonner E, Flint DJ, Selbert S, Takeda K, Akira S, Clarke AR, Watson CJ. Suppression of epithelial apoptosis and delayed mammary gland involution in mice with a conditional knockout of Stat3. Genes Dev. 1999; 13:2604–2616. [PubMed: 10521404]

Colbert LH, Davis JM, Essig DA, Ghaffar A, Mayer EP. Tissue expression and plasma concentrations of TNFalpha, IL-1beta, and IL-6 following treadmill exercise in mice. Int J Sports Med. 2001; 22:261–267. [PubMed: 11414667]

Cotman CW, Berchtold NC, Christie LA. Exercise builds brain health: key roles of growth factor cascades and inflammation. Trends Neurosci. 2007; 30:464–472. [PubMed: 17765329]

Darnell JE, Kerr IM, Stark GR. Jak-STAT pathways and transcriptional activation in response to IFNs and other extracellular signaling proteins. Science. 1994; 264:1415–1421. [PubMed: 8197455]

Ding Y-H, Mrizek M, Lai Q, Wu Y, Reyes R Jr, Li J, Davis WW, Ding Y. Exercise preconditioning reduces brain damage and inhibits TNF-α receptor expression after hypoxia/reoxygenation: An in vivo and in vitro study. Curr Neurovasc Res. 2006; 3:263–271. [PubMed: 17109621]

Droste SK, Chandramohan Y, Hill LE, Linthorst ACE, Reul JMHM. Voluntary exercise impacts on the rat hypothalamic-pituitary-adrenocortical axis mainly at the adrenal level. Neuroendocrinol. 2007; 86:26–37.

Eskes C, Juillerat-Jeanneret L, Leuba G, Honnegger P, Monnet-Tschudi F. Involvement of microglia-neuron interactions in the tumor necrosis factor-alpha release, microglial activation, and neurodegeneration induced by trimethyltin. J Neurosci Res. 2003; 71:583–590. [PubMed: 12548715]

Fiedorowicz A, Figiel I, Kaminska B, Zaremba M, Wilk S, OderFeld-Nowak B. Dentate granule neuron apoptosis and glia activation in murine hippocampus induced by trimethyltin exposure. Brain Res. 2001; 912:116–127. [PubMed: 11532427]

Figiel I, Dzwonek K. TNFalpha and TNF receptor 1 expression in the mixed neuronal-glial cultures of hippocampal dentate gyrus exposed to tlutamate or trimethyltin. Brain Res. 2007; 1131:17–28. [PubMed: 17161388]

Geloso MC, Vercelli A, Corvino V, Repici M, Boca M, Haglid K, Zelano G, Michetti F. Cyclooxygenase-2 and caspase 3 expression in trimethyltin-induced apoptosis in the mouse hippocampus. Exp Neurol. 2002; 175:152–160. [PubMed: 12009767]

Hacker H, Karin M. Regulation and function of IKK and IKK-related kinases. Sci STKE. 2006; 357 re13.

Harry GJ, Bruccoleri A, Lefebvre d'Hellencourt C. Differential modulation of hippocampal chemical-induced injury response by ebselen, pentoxifylline, and TNF-alpha- IL-1alpha-, and IL-6-neutralizing antibodies. J Neurosci Res. 2003; 73:526–536. [PubMed: 12898537]

Harry GJ, Tyler K, Lefebvre d'Hellencourt C, Tilson HA, Maier WE. Morphological alterations and elevations in tumor necrosis factor-alpha, interleukin (IL)-1alpha, and IL-6 in mixed glia cultures following exposure to trimethyltin: modulation by proinflammatory cytokine recombinant proteins and neutralizing antibodies. Toxicol Appl Pharmacol. 2002; 180:205–218. [PubMed: 12009860]

Harry GJ, Lefebvre d'Hellencourt C, McPherson CA, Funk JA, Aoyama M, Wine RN. Tumor necrosis factor p55 and p75 receptors are involved in chemical-induced apoptosis of dentate granule neurons. J Neurochem. 2008; 106:281–298. [PubMed: 18373618]

Heppner FL, Roth K, Nitsch R, Hailer NP. Vitamin E induces ramification and downregulation of adhesion molecules in cultured microglial cells. Glia. 1998; 22:180–188. [PubMed: 9537838]

Hirota H, Kiyama H, Kishimoto T, Taga T. Accelerated nerve regeneration in mice by upregulated expression of interleukin (IL)6 and IL-6 receptor after trauma. J Exp Med. 1996; 183:2627–2634. [PubMed: 8676083]

Ihle JN. STATs: Signal transducers and activators of transcription. Cell. 1996; 84 331-143.

Ito CY, Adey N, Bautch VL, Baldwin AS Jr. Structure and evolution of the human IKBA gene. Genomics. 1995; 29:490–495. [PubMed: 8666399]

Joels M. Role of corticosteroid hormones in the dentate gyrus. Prog Brain Res. 2007; 163:355–370. [PubMed: 17765729]

Jonsdottir IH, Schjerling P, Ostrowski K, Asp S, Richter EA, Pedersen BK. Muscle contractions induce interleukin-6 mRNA production in rat skeletal muscles. J Physiol. 2000; 528(Pt 1):157–163. [PubMed: 11018114]

Karin M, Ben-Neriah Y. Phosphorylation meets ubiquitination: the control of NF-[kappa]B activity. Annu Rev Immunol. 2000; 18:621–663. [PubMed: 10837071]

Kramer AF, Erickson KI. Capitalizing on cortical plasticity: influence of physical activity on cognition and brain function. Trends Cogn Sci. 2007; 11:342–348. [PubMed: 17629545]

Lee DK, Carrasco J, Hidalgo J, Andrews GK. Identification of a signal transducer and activator of transcription (STAT) binding site in the mouse metalothionein-1 promoter involved in interleukin-6-induced gene expression. Biochem J. 1999; 337:59–65. [PubMed: 9854025]

Little AR, Sriram K, O'Callaghan JP. Corticosterone regulates expression of CCL2 in the intact and chemically injured hippocampus. Neurosci Lett. 2006; 399:162–166. [PubMed: 16504399]

Micheau O, Lens S, Gaide O, Alevizopoulos K, Tschopp J. NF-kappaB signals induce the expression of c-FLIP. Mol Cell Biol. 2001; 21:5299–5305. [PubMed: 11463813]

Matthys P, Mitera T, Heremans H, Van Damme J, Billiau A. Anti-gamma interferon and anti-interleukin-6 antibodies affect staphylococcal enterotoxin B-induced weight loss, hypoglycemia, and cytokine release in D-galactosamine-sensitized and unsensitized mice. Infection and Immunity. 1995; 63:1158–1164. [PubMed: 7890366]

Mizuhara H, O'Neill E, Seki N, Ogawa T, Kusunoki C, Otsuka K, Satoh S, Niwa M, Senoh H, Fujiwara H. T cell activation-associated hepatic injury: mediation by tumor necrosis factors and protection by interleukin 6. Jour Exper Med. 1994; 179:1529–1537. [PubMed: 8163936]

Molinero A, Penkowa M, Hernandez J, Camats J, Giralt M, Lago N, Carrasco J, Campbell IL, Hidalgo J. Metallothionein-1 overexpression decreases brain pathology in transgenic mice with astrocyte-targeted expression of interleukin 6. J Neuropathol Exp Neurol. 2003; 62:315–328. [PubMed: 12638735]

Morita Y, Yanagida D, Shintani N, Ogita K, Nishiyama N, Tsuchida R, Hashimoto H, Baba A. Lack of trimethyltin (TMT)-induced elevation of plasma corticosterone in PACAP-deficient mice. Ann NY Acad Sci. 2006; 1070:450–456. [PubMed: 16888208]

Nakajima K, Yamanaka Y, Nakae K, Kojima H, Ichiba M, Kiuchi N, Kitaoka T, Fukada T, Hibi M, Hirano T. A central role for STAT3 in IL-6 induced regulation of growth and differentiation in M1 leukemia cells. EMBO J. 1996; 15:3651–3658. [PubMed: 8670868]

Nichol KE, Poon WW, Parachikova AI, Cribbs DH, Glabe CG, Cotman CW. Exercise alters the immune profile in Tg2576 Alzheimer mice toward a response coincident with improved cognitive performance and decreased amyloid. J Neuroinflam. 2008; 5:13.

Nybo L, Nielsen B, Pedersen BK, Secher NH. Interleukin-6 release from the human brain during prolonged exercise. J Physiol. 2002; 542:991–995. [PubMed: 12154196]

Parachikova A, Nichol KE, Cotman CW. Short-term exercise in aged Tg2576 mice alters neuroinflammation and improves cognition. Neurobiol Dis. 2008; 30:121–129. [PubMed: 18258444]

Penkowa M, Giralt M, Carrasco J, Hadberg H, Hidalgo J. Impaired inflammatory response and increased oxidative stress and neurodegeneration after brain injury in interleukin-6-deficient mice. Glia. 2000; 32:271–285. [PubMed: 11102968]

Penkowa M, Giralt M, Lago N, Camats J, Carrasco J, Hernandez J, Molinero A, Campbell IL, Hidalgo J. Astrocyte-targeted expression of IL-6 protects the CNS against a focal brain injury. Exp Neurol. 2003; 181:130–148. [PubMed: 12781987]

Petersen AM, Pedersen BK. The role of IL-6 in mediating the anti-inflammatory effects of exercise. J. Physiol. Pharmacol. 2006; 57 Suppl 10:43–51. [PubMed: 17242490]

Pedersen BK, Fischer CP. Physiological roles of muscle-derived interleukin-6 in response to exercise. Curr Opin Clin Nutri Metab Care. 2007; 10:265–271.

Rasmussen P, Vedel JC, Olesen J, Adser H, Pedersen MV, Hart E, Secher NH, Pilegaard H. In humans IL-6 is released from the brain during and after exercise and paralleled by enhanced IL-6 mRNA expression in the hippocampus of mice. Acta Physiol. 2010

Reese BE, Krissinger D, Yun JK, Billingsley ML. Elucidation of stannin function using microarray analysis: implications for cell cycle control. Gene Expr. 2006; 13:41–52. [PubMed: 16572589]

Reich NC. STAT dynamics. Cytokine Growth Factor Rev. 2007; 18:511–518. [PubMed: 17683973]

Rowley M, Van Ness B. Activation of N-ras and K-ras induced by interleukin-6 in a myeloma cell line: implications for disease progression and therapeutic response. Oncogene. 2002; 21:8769–8775. [PubMed: 12483530]

Schubert KO, Neumann T, Schnell O, Zhi Q, Steup A, Hofmann HD, Kirsch M. Activation of STAT3 signaling in axotomized neurons and reactive astrocytes after fimbria-fornix transection. Exp Brain Res. 2005; 165:520–531. [PubMed: 15991029]

Shuto M, Higuchi K, Sugiyama C, Yoneyama M, Kuramoto N, Nagashima R, Kawada K, Ogita K. Endogenous and exogenous glucocorticoids prevent trimethyltin from causing neuronal degeneration of the mouse brain in vivo: involvement of oxidative stress pathways. J Pharmacol Sci. 2009; 110:424–436. [PubMed: 19602844]

Starkie R, Ostrowski SR, Jauffred S, Febbraio M, Pedersen BK. Exercise and IL-6 infusion inhibit endotoxin-induced TNF-α production in humans,". The FASEB Jour. 2003; 17:884–886.

Swartz KR, Liu F, Sewell D, Schochet T, Campbell I, Sandor M, Fabry Z. Interleukin-6 promotes post-traumatic healing in the central nervous system. Brain Res. 2001; 896:86–95. [PubMed: 11277977]

Taoufik E, Valable S, Muller GJ, Roberts ML, Divoux D, Tinel A, Voulgari-Kokota A, Tseveleki V, Altruda F, Lassmann H, Petit E, Probert L. FLIP(L) protects neurons against in vivo ischemia and in vitro glucose deprivation-induced cell death. J Neurosci. 2007; 27:6633–6646. [PubMed: 17581950]

Tilg H, Trehu E, Atkins MB, Dinarello CA, Mier JW. Interleukin-6 (IL-6) as an anti-inflammatory cytokine: induction of circulating IL-1 receptor antagonist and soluble tumor necrosis factor receptor p55. Blood. 1994; 83:113–118. [PubMed: 8274730]

Toggas SM, Krady JK, Billingsley ML. Molecular neurotoxicology of trimethyltin: identification of stannin, a novel protein expressed in rimethyltin-sensitive cells. Mol Pharmacol. 1992; 42:44–56. [PubMed: 1635553]

Tsakiri N, Kimber I, Rothwell NJ, Pinteaux E. Mechanisms of interleukin-6 synthesis and release induced by interleukin-1 and cell depolarization in neurons. Mol Cell Neurosci. 2008; 37:110–118. [PubMed: 17933551]

van Praag H, Shubert T, Zhao C, Gage FH. Exercise enhances learning and hippocampal neurogenesis in aged mice. J Neurosci. 2005; 25:8680–8685. [PubMed: 16177036]

Weng L, Dai H, Zhan Y, He Y, Stepaniants SB, Bassett DE. Rosetta error model for gene expression analysis. Bioinformatics. 2006; 22:1111–1121. [PubMed: 16522673]

Wesche H, Henzel WJ, Shillinglaw W, Li S, Cao Z. MyD88: an adapter that recruits IRAK to the IL-1 receptor complex. Immunity. 1997; 7:837–847. [PubMed: 9430229]

Wilms H, Hartmann D, Sievers J. Ramification of microglia, monocytes and macrophages in vitro: influences of various epithelial and mesenchymal cells and their conditioned media. Cell Tissue Res. 1997; 287:447–458. [PubMed: 9023076]

Xia X, Hofmann H-D, Deller T, Kirsch M. Induction of STAT3 signaling in activated astrocytes and sprouting neurons following entorhinal cortex lesion in adult rats. Mol Cell Neurosci. 2002; 21:379–392. [PubMed: 12498781]

Yang J, Chatterjee-Kishore M, Staugaitis SM, Nguyen H, Schlessinger K, Levy DE, Stark GR. Novel roles of unphosphorylated STAT3 in oncogenesis and transcriptional regulation. Cancer Res. 2005; 65:939–947. [PubMed: 15705894]

Yang J, Liao X, Agarwal MK, Barnes L, Auron PE, Stark GR. Unphosphorylated STAT3 accumulates in response to IL-6 and activates transcription by binding to NFkB. Genes Develop. 2007; 21:1396–1408. [PubMed: 17510282]

Yoneyama M, Nishiyama N, Shuto M, Suglyama C, Kawada K, Seko K, Nagashima R, Ogita K. In vivo depletion of endogenous glutathione facilitates trimethyltin-induced neuronal damage in the dentate gryus of mice by enhancing oxidative stress. Neurochem Int. 2008; 52:761–769. [PubMed: 17949856]

Zhong J, Dietzel ID, Wahle P, Kopf M, Heumann R. Sensory impairments and delayed regeneration of sensory axons in interleukin-6-deficient mice. J Neurosci. 1999; 19:4305–4313. [PubMed: 10341234]

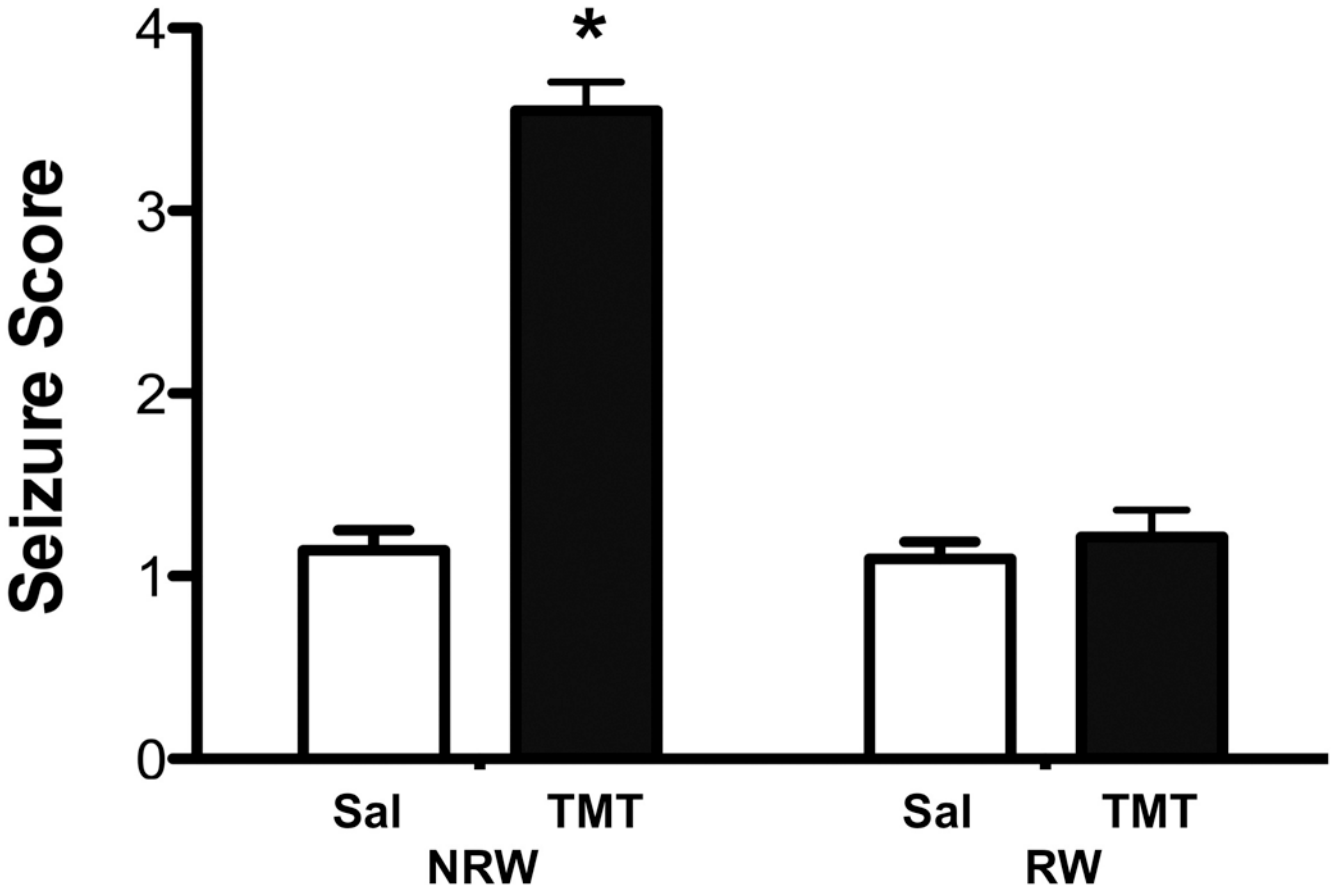

Figure 1.
TMT induced tremors and seizures in CD-1 male mice at 24hrs post-injection. Data represent seizure scores (mean ± 95% confidence interval) of mice allowed 2wks free access to a running wheel (RW) or maintained in normal home cage environment (NRW) 24hrs following an ip injection of either saline or trimethyltin (TMT, 2.4 mg/kg). * indicates statistically significant as compared to saline controls for each housing condition as determined by Mann-Whitney (n=42).

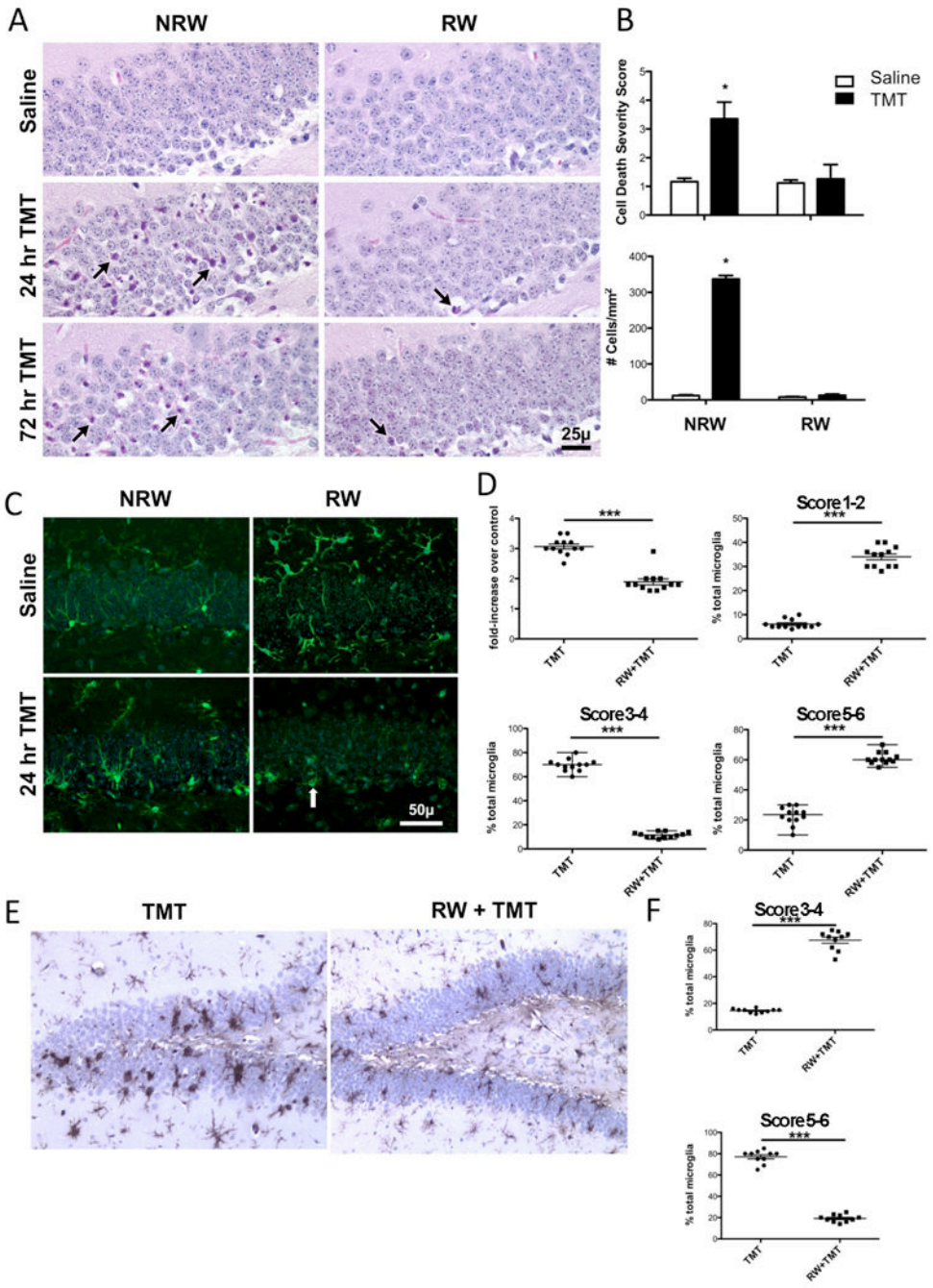

Figure 2.

(A) Representative hematoxylin and eosin (H&E) staining in the suprapyramidal blade of the dentate gyrus of mice allowed 2wks free access to a running wheel (RW) or maintained in normal home cage environment (NRW) under saline or at 24 and 72hrs following an ip injection of trimethyltin (TMT, 2.4 mg/kg). Eosin+ neurons (arrows) were detected throughout the blade in the NRW+TMT mice. Scale bar = 25µm. (B) Data represents the neuronal death severity score (mean ± 95% CI) and number of eosin+ cells (mean ± SEM) within a region of interest (ROI) within the granule cell layer (GCL) as described in Methods. * indicates statistical significant as determined by Mann-Whitney U test as compared to the NRW saline group (n=42). (C) Representative images of

immunofluorescent staining for Iba-1+ microglia within the suprapyramidal blade of the dentate gyrus. Scale bare = 50 μm. (D) Fold-increase in number of microglia cells within ROI for each exercise group dosed with TMT relative to controls. Morphological phenotype score of each group as described in Methods as a % of the total microglia (mean ± SEM). *** indicates statistical significance ($p<0.0001$) as determined by Mann-Whitney U. (n=12). (E) Representative image of $IB4^{+}$ microglia detected with DAB (hematoxylin counterstain) at 72hrs post-TMT in sedentary mice (NRW+TMT) and mice allowed 2wks access to RW (RW+TMT). (F) Data represent scatter plots of phenotype scores as a % of total microglia at 72hrs post-TMT indicating a progression to amoeboid microglia in the NRW+TMT group. *** indicates statistically significant ($p<0.0001$) as determined by Mann-Whitney U test.

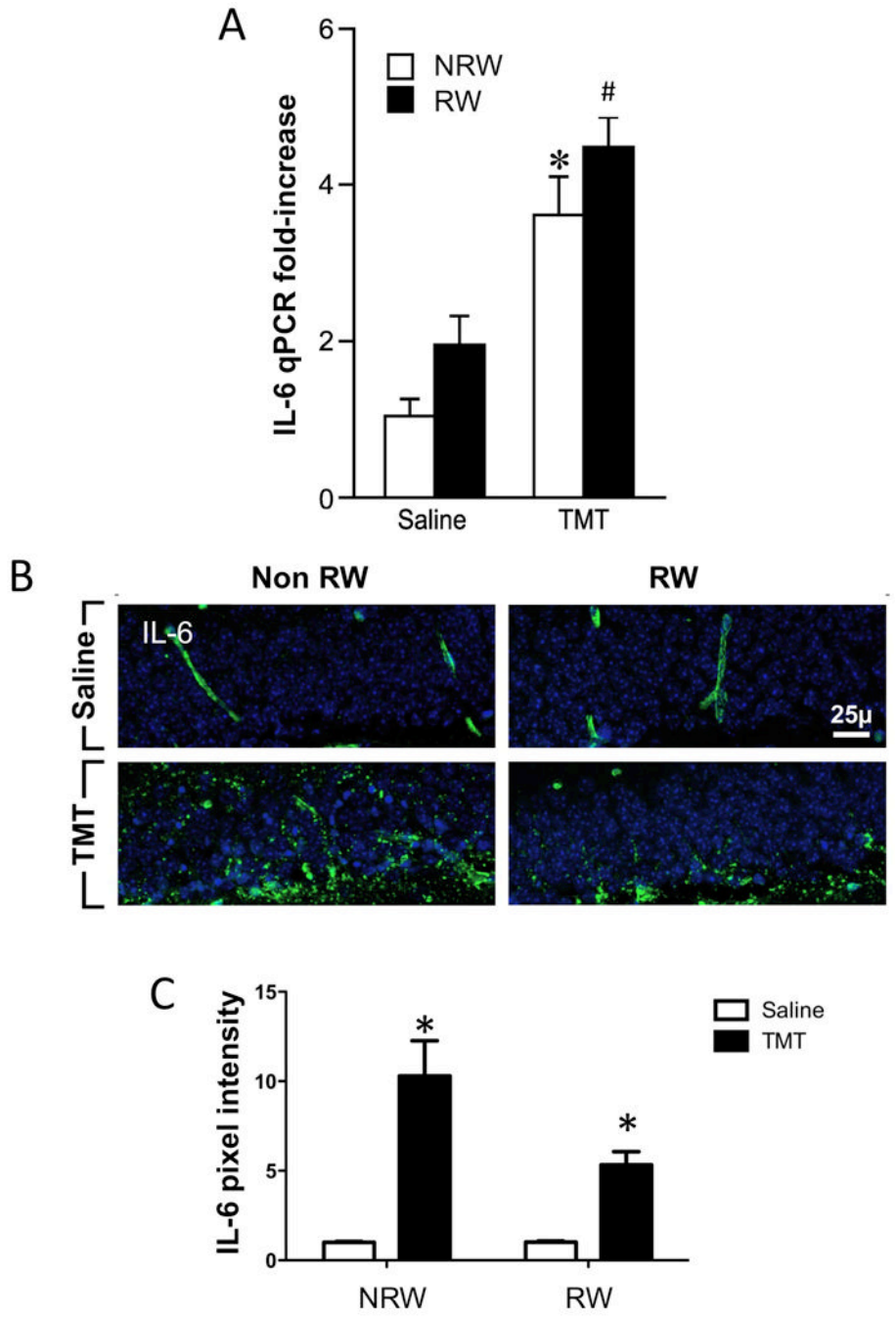

Figure 3.

(A) Quantitative real-time PCR (qRT-PCR) for IL-6 in the hippocampus of mice. (B) Immunoreactivity of IL-6 within the dentate granule cell layer (GCL). (C) estimation of protein within the GCL as determined by fluorescent pixels within a defined region of interest. Mice were allowed 2wks free access to a running wheel (RW) or maintained in normal home cage environment (NRW) followed by an ip injection of either trimethyltin (TMT, 2.4 mg/kg) or saline (1ml/kg body wt) and hippocampal tissue collected 24hrs post injection. Data represents mean ±SEM. * indicates statistical significance as compared to NRW control; # as compared to RW control. Scale bar = 25µm.

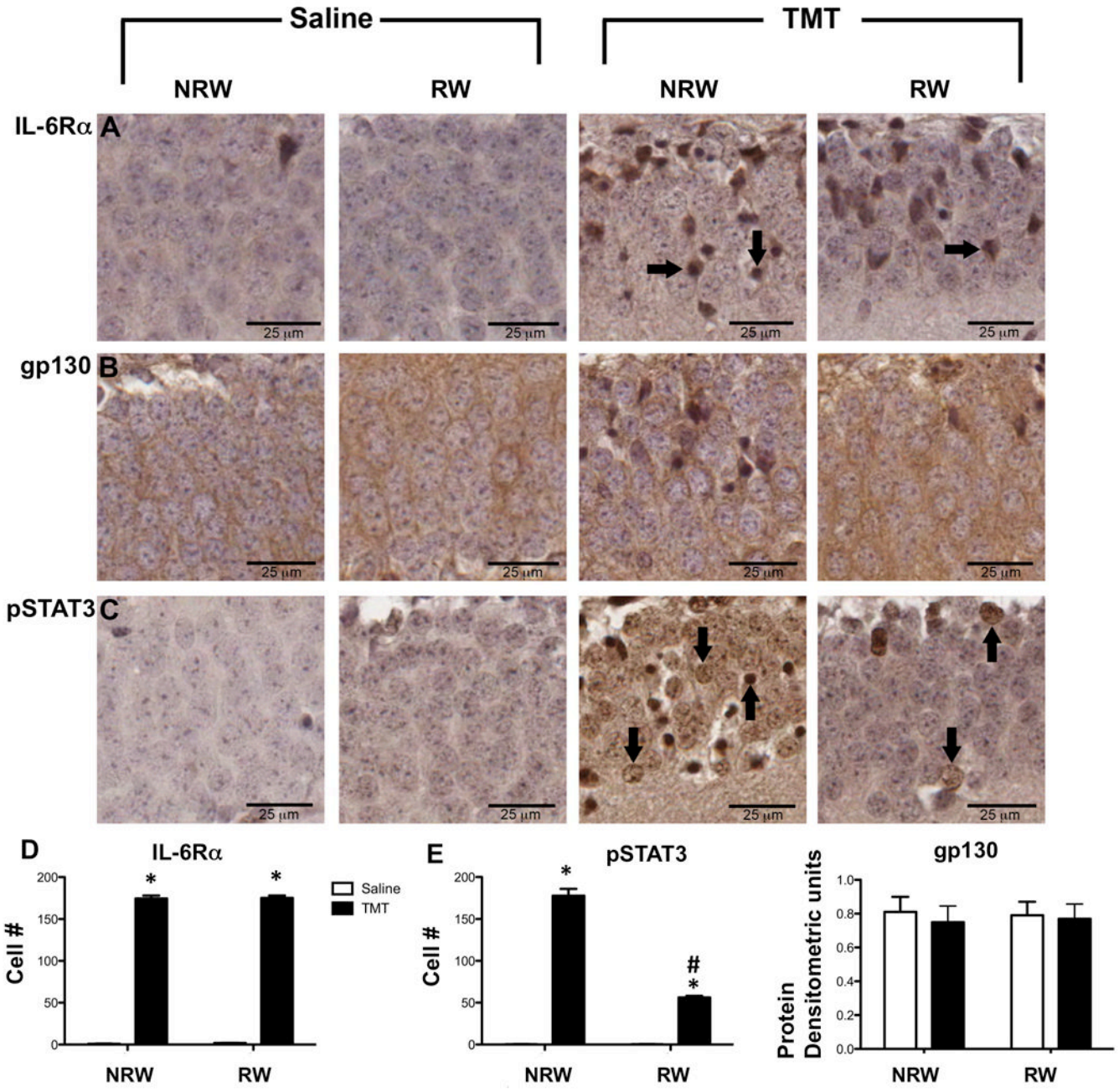

Figure 4.

Representative immunohistochemistry for (A) IL-6Rα, (B) gp130, (C) pSTAT3 in the suprapyramidal blade of the GCL of mice exposed to 2wks of running wheel (RW) or normal home cage (NRW) and injected with either saline or trimethyltin (TMT; 2.4mg/kg, ip). Samples represent changes occurring 24hrs post-injection. Arrows indicate immunopositive neurons. Scale bar = 25μm. (D) estimated number of IL-6Rα within the GCL. (E) estimated number of pSTAT3 immunopositive cells within the GCL as described in Methods. (F) densitometric units of gp130 protein levels as determined by Western blot. Data represents mean ± SEM (n=7). * indicates statistically significant as compared to saline

as determined by Bonferroni multiple comparisons following a 2×2 ANOVA. # indicates statistically significant as compared to NRW+TMT.

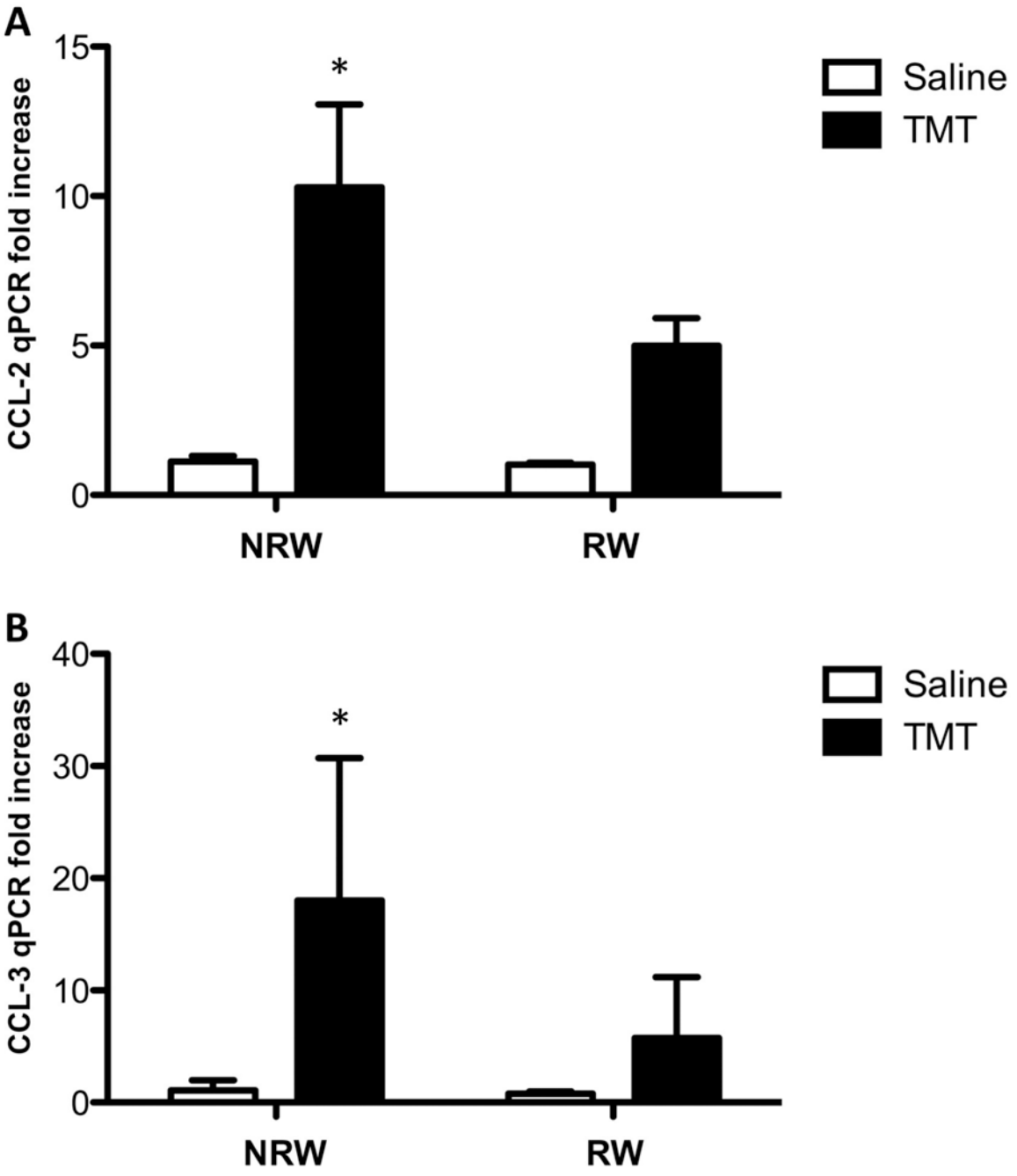

Figure 5.

Quantitative PCR of (A) CCL-2 and (B) CCL-3 in the hippocampus of mice allowed 2wks free access to a running wheel (RW) or maintained in home care (NRW) followed by an injection of TMT (2.4 mg/kg ip) or saline as examined 24hrs post injection. Data are presented a mean fold increase (± SD) over the average saline/NRW control for each mRNA transcript (n=6). * indicates significantly different as compared to the NRW control group as determined by Bonferroni following a 2×2 ANOVA.

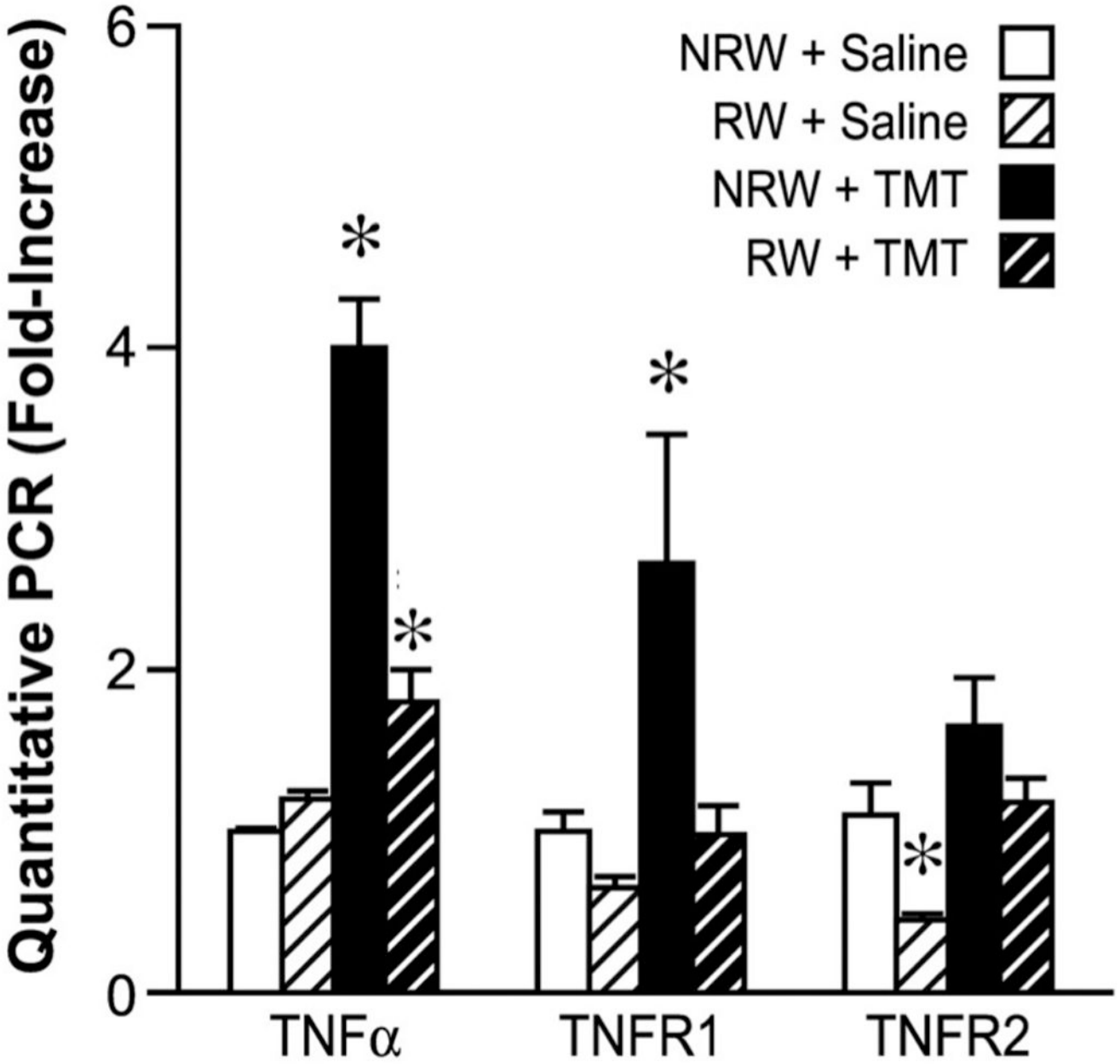

Figure 6.

Quantitative RT-PCR for TNFα, TNFR1, and TNFR2 in the hippocampus. Mice were allowed 2wks free access to a running wheel (RW) or maintained in normal home cage environment (NRW) followed by an ip injection of either trimethyltin (TMT, 2.4 mg/kg) or saline (1ml/kg body wt) and hippocampal tissue collected 24hrs post injection. Data represents mean ± SD (n=6) * indicates significantly different as compared to the NRW control as determined by Bonferroni multiple comparisons following a significant 2×2 ANOVA.

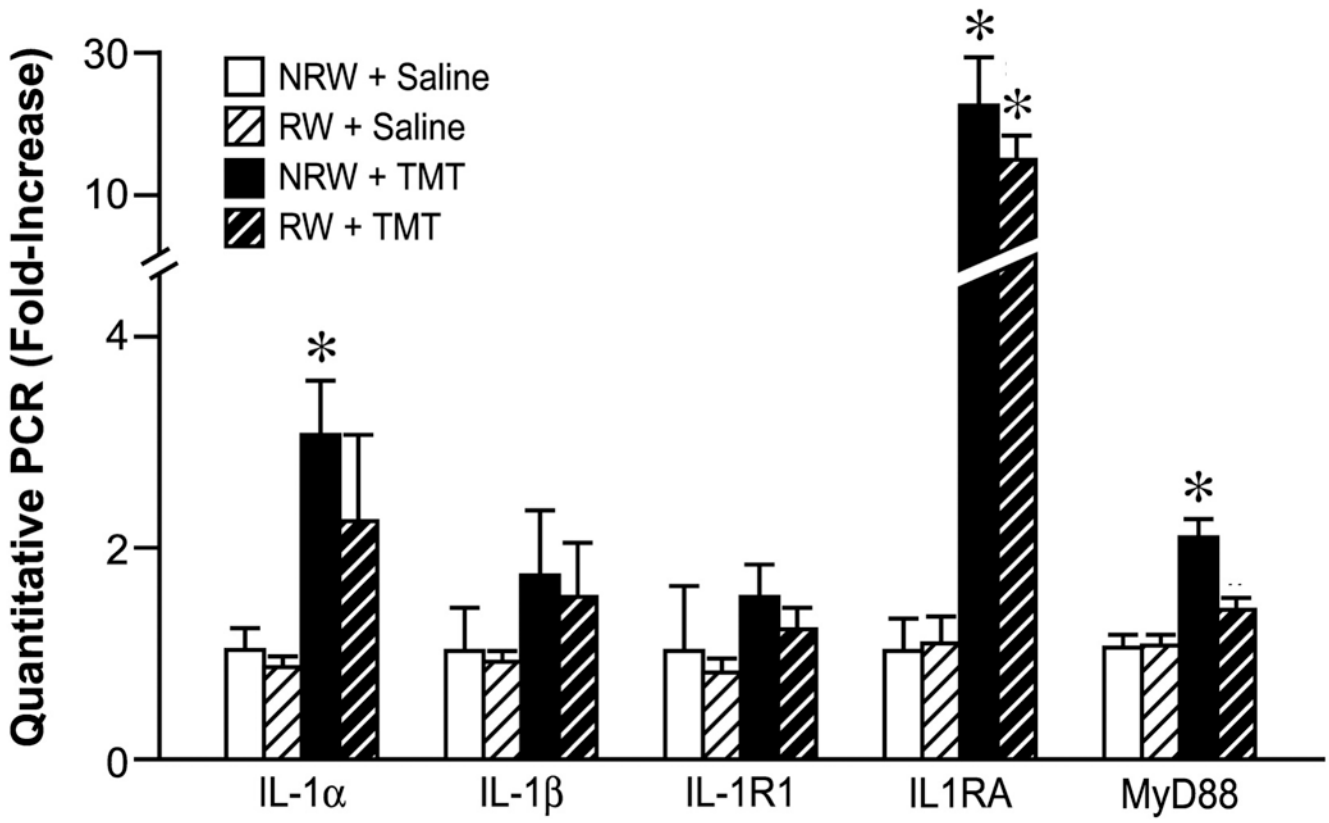

Figure 7.

Quantitive RT-PCR of genes associated with interleukin-1 signaling in the hippocampus. Mice were allowed 2wks free access to a running wheel (RW) or maintained in normal home cage environment (NRW) followed by an ip injection of either trimethyltin (TMT, 2.4 mg/kg) or saline (1ml/kg body wt) and hippocampal tissue collected 24hrs post injection. Data are presented as a mean fold-change (± SD) over the average saline/NRW control for each mRNA transcript (n=6). * indicates significantly different as compared to the NRW control as determined by Bonferroni following a 2×2 ANOVA.

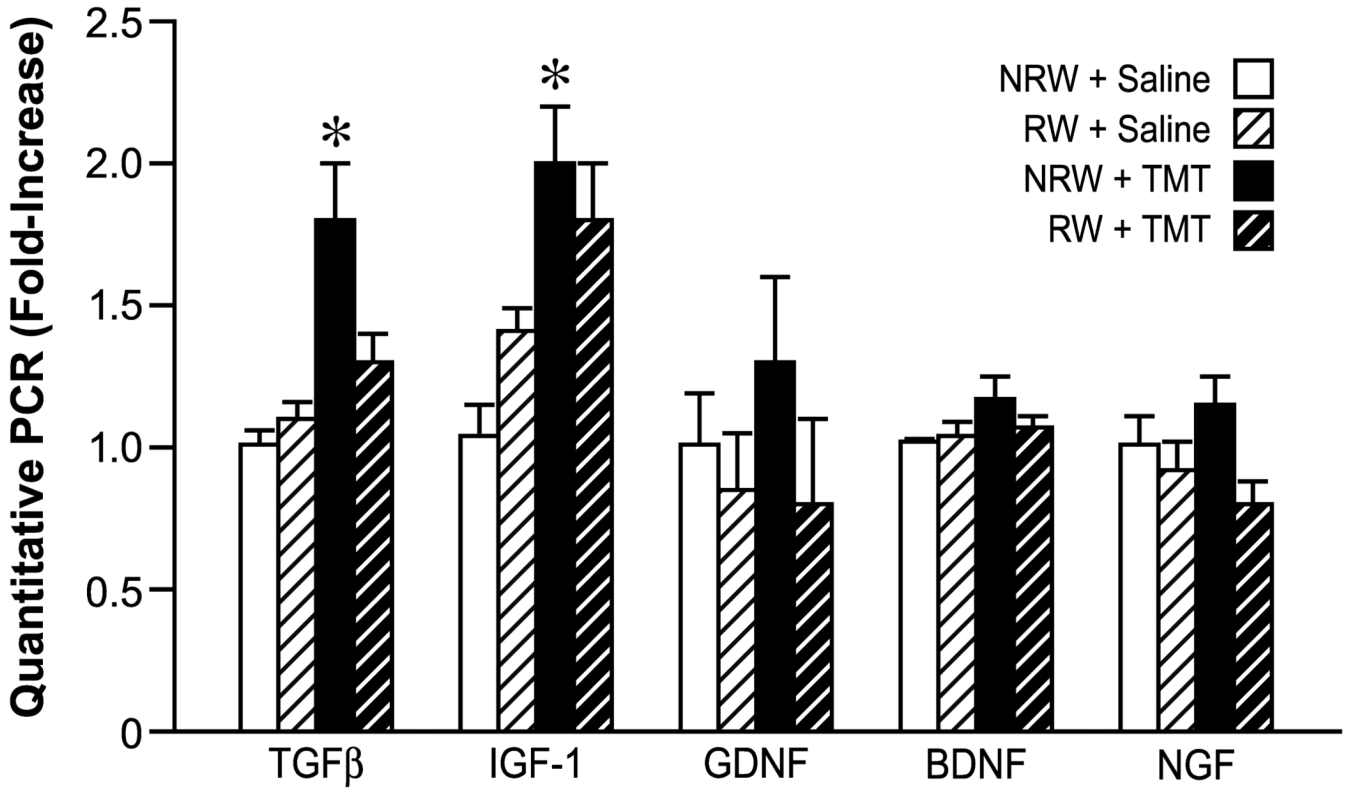

Figure 8.

Quantitative RT-PCR of genes associated with neurotrophic factors in the hippocampus. Mice were allowed 2wks free access to a running wheel (RW) or maintained in normal home cage environment (NRW) followed by an ip injection of either trimethyltin (TMT, 2.4 mg/kg) or saline (1ml/kg body wt) and hippocampal tissue collected 24hrs. Data are presented as a mean fold-change (mean ±SD) over the average saline/NRW control for each mRNA transcript (n=6). * indicates significantly different ($p<0.05$) as compared to the NRW control as determined by Bonferroni following a 2×2 ANOVA.

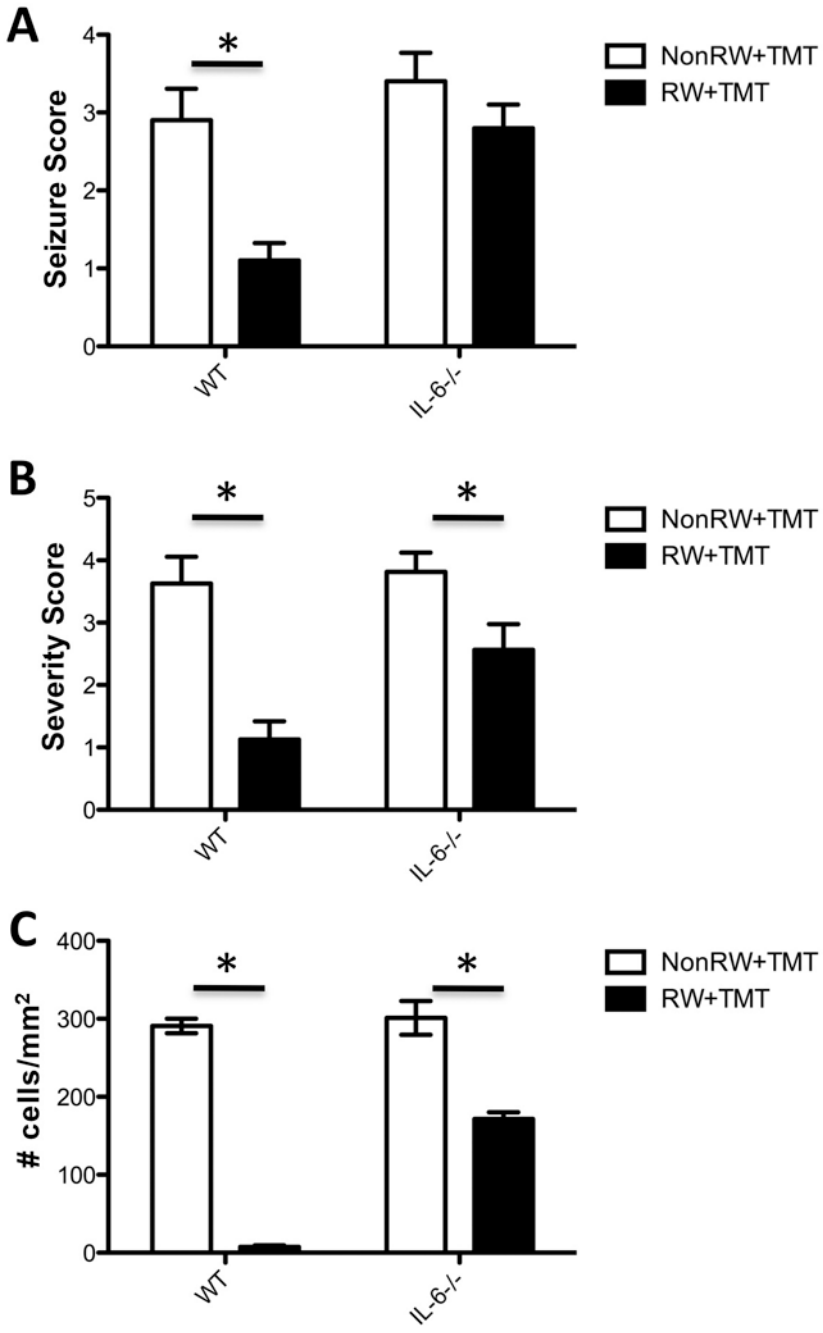

Figure 9.

(A) seizure score (B) cell death severity score, and (C) number of eosin+ cells within a defined ROI of the GCL 24hrs post-TMT injection (2.4 mg/kg body wt, ip) in B6129SF2/J (WT) and IL-6−/− mice. Mice were maintained under individual housing conditions (NRW) or allowed 2wks free access to a running wheel (RW) prior to the TMT injection. Scoring data represents mean ± 95% CI; * indicates statistical significance as compared to NRW group within genotype as determined by (A,B) Mann Whitney U and (C) Bonferroni post-hoc analysis following 2×2 ANOVA.

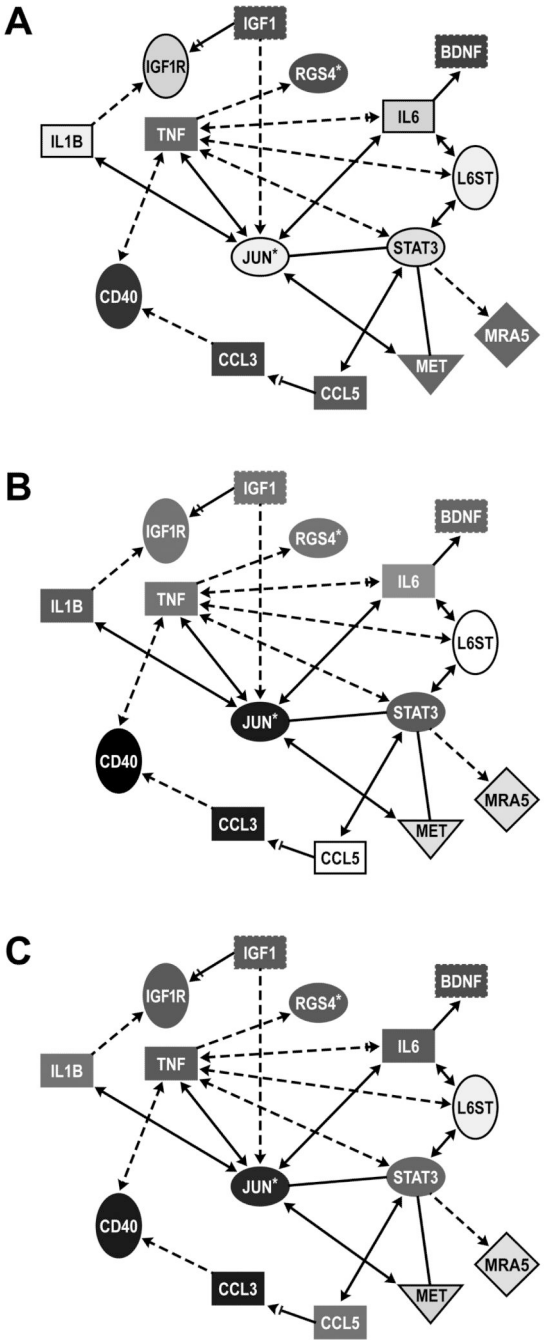

Figure 10.

Focused network analysis of connectivity between injury and neuroprotection pathways in the hippocampus. Using Ingenuity Knowledge Based function, we examine the connectivity between genes related to the IL-6 and STAT3 pathways under each condition as outlined in the Methods section. Entries with white lettering signify upregulation and entries with black lettering signifies downregulation, with shade of color reflective of level of difference.

A. Comparison between mice allowed 2wks voluntary exercise in a running wheel (RW) with those maintained in the home cage (NRW) suggested upregulation of unphosphorylated STAT3 targets (CCL-5, MET, and MRAS) in RW mice.

B. Comparison between mice injected with saline or TMT (2.4 mg/kg, ip, 24hrs) maintained in the home care (NRW) suggesting an upregulation of IL-6 and STAT3 yet, a downregulation of CCL-5, MET, and MRAS.
C. Comparison between mice allowed 2wks access to RW prior to an injection with TMT as compared to saline NRW controls suggesting an upregulation of IL-6 and CCL-5.
*statistical significance $p<0.001$. Pathways were built using Ingenuity connect function on molecules known to be associated injury and protection based on current literature.

Brain Behav Immun. Author manuscript; available in PMC 2012 August 1.

TABLE 1

Genes changed in the Biocarta cell death pathway

Sequence Code	Primary Sequence Name	Accession #	Non-Running Wheel Untreated vs. TMT Treated		Running Wheel Untreated vs. TMT Treated	
			Fold Change	*P*-Value	Fold Change	*P*-Value
1449731_s_at	AI462015	AI462015	**1.68**	**6.90E-04**	*1.13*	*4.04E-01*
1450223_at	Apaf1	NM_009684	*1.41*	*1.30E-01*	*1.78*	*9.14E-03*
1426165_a_at	Casp3	D86352	**3.74**	**1.00E-05**	*2.01*	*1.13E-01*
1449839_at	Casp3	BG070529	**3.64**	**5.94 E-08**	*2.48*	*5.06E-03*
1424996_at	Cflar	BC023121	**1.87**	**5.00E-04**	*1.56*	*3.93E-02*
1451383_a_at	Chuk; IKK-alpha	BC018243	**1.38**	**7.56E-07**	*1.21*	*7.51E-03*
1422484_at	Cycs	NM_007808	**−1.23**	**5.65E-17**	**−1.18**	**1.18E-07**
1437051_at	Dffb	AV300013	*1.63*	*2.26E-03*	**2.07**	**3.00E-05**
1448306_at	Nfkbia	NM_010907	**2.10**	**2.00E-05**	*1.48*	*2.80E-02*
1438157_s_at	Nfkbia	BB096843	**1.99**	**3.38E-06**	*1.21*	*2.26E-01*
1422231_a_at	Tnfrsf25	AF329969	1.56	*3.21E-01*	*2.41*	*1.41E-03*
1422231_a_at	Tnfrsf25	AF329969	**1.50**	**5.80E-04**	*1.38*	*7.49E-03*

*bolded values represent those that meet the significance cutoff set at 1.2 fold change and p-value <0.0001.

P-value is presented in exponential (E) form

TABLE 2

Genes differentially changed on Biocarra pathways for inflammation and phagocytosis

Sequence Code	Primary Sequence Name	Accession #	Non-Running Wheel Untreated vs. TMT Treated		Running Wheel Untreated vs. TMT Treated	
			Fold Change	*P*-Value	Fold Change	*P*-Value
1417381_at	C1qa	NM_007572	**2.41**	**5.00E-05**	**2.29**	**1.00E-04**
1434366_x_at	C1qb	AW227993	*1.86*	*5.07E-03*	**1.92**	**9.10E-04**
1417063_at	C1qb	NM_009777	**2.22**	**6.91 E-06**	**2.27**	**3.70E-04**
1426165_a_at	Casp3	D86352	**3.74**	**1.00E-05**	*2.01*	*1.13E-01*
1449839_at	Casp3	BG070529	**3.64**	**5.94E-08**	*2.48*	*5.06E-03*
1451383_a_at	Chuk; IKK-alpha	BC018243	**1.38**	**7.56E-07**	*1.21*	*7.51E-03*
1437051_at	Dffb	AV300013	*1.63*	*2.26E-03*	**2.07**	**3.00E-05**
1423100_at	Fos	AV026617	*−1.01*	*9.81 E-01*	**2.49**	**2.00E-05**
1448694_at	Jun	NM_010591	**2.69**	**1.69E-18**	**2.25**	**4.55E-12**
1417409_at	Jun	NM_010591	**2.80**	**4.81 E-23**	**2.65**	**3.16E-15**
1426850_a_at	Map2k6	BB261602	**−2.37**	**2.05E-06**	*−1.36*	*4.81E-02*
1449731_s_at	Nfκbia	AI462015	**1.68**	**6.90E-04**	*1.13*	*4.04E-01*
1438157_s_at	Nfκ-bia	BB096843	**1.99**	**3.38E-06**	*1.21*	*2.26E-01*
1448306_at	Nfκbia	NM_010907	**2.10**	**2.00E-05**	*1.48*	*2.80E-02*
1423047_at	Tollip	BB400304	**1.50**	**5.80E-04**	*1.38*	*7.49E-03*

*bolded values represent those that meet the significance cutoff set at 1.2 fold change and p-value <0.0001.

P-value is presented in exponential (E) form

Brain Behav Immun. Author manuscript; available in PMC 2012 August 1.

Table 3

Genes changed in the Biocarta IL-6 pathway

Sequence Code	Primary Sequence Name	Accession #	Non-Running Wheel Untreated vs. TMT Treated		Running Wheel Untreated vs. TMT Treated	
			Fold Change	*P*-Value	Fold Change	*P*-Value
1451225_at	2700084A17Rik	BC003980	**1.23**	**4.00E-05**	**1.23**	**5.50E-04**
1423100_at	Fos	AV026617	*−1.01*	*9.81E-01*	**2.49**	**2.00E-05**
1422407_s_at	Hras1	NM_008284	**−1.50**	**3.60E-04**	*−1.29*	*5.58E-03*
1448694_at	Jun	NM_010591	**2.69**	**1.69E-18**	**2.25**	**4.55E-12**
1417409_at	Jun	NM_010591	**2.80**	**4.81 E-23**	**2.65**	**3.16E-15**
1418255_s_at	Srf	BI662291	**−1.33**	**2.00E-05**	*−1.17*	*1.43E-02*
1426587_a_at	Stat3	AI325183	**1.47**	**7.90E-04**	*1.22*	*9.38E-02*
1451383_a_at	Chuk, IKK-alpha	BC018243	**1.38**	**7.56E-07**	*1.21*	*7.51E-03*

* bolded values represent those that meet the significance cutoff set at 1.2 fold change and p-value <0.0001.

P-value is presented in exponential (E) form